



Tectonic and structural influences on the Dulung River system in the southwestern fringe of Bengal Basin

Subrata Jana¹

Received: 26 April 2021 / Accepted: 15 December 2021 / Published online: 3 January 2022
© Saudi Society for Geosciences 2021

Abstract

The tectonic and structural influences on the hydrogeomorphological adjustment of the Dulung River system in the southwestern fringe of Bengal Basin have been assessed using satellite images and on-field investigations. The river course is more altered and adjusted with the deformed Quaternary formations within the Chotanagpur foothill fault and Medinipur-Farakka fault (MFF) zone. The adjustments of the drainage system are reflected by the analysis of morphotectonic, geological, morphometric, and hydrogeomorphological attributes coupled with the channel patterns and forms of profiles. The tectonic potentiality index-based four tectonic potential zones have been estimated considering the ten morphotectonic and hydrogeomorphological variables, i.e., basement depth, Bouguer gravity anomaly, isobase, hydraulic gradient, lineament density, flow turn angle, sinuosity index, palaeo-channel density, relation declivity extension index (RDE-index), and transverse topographic symmetry factor (T-index). The four stages of river adjustment are associated within the middle-lower basin area. The river confluences gradually shifted in the upstream direction, maintaining about 10–15 km inter-confluence distance. The recent and palaeo-courses of the river Dulung and Subarnarekha continuously shifted towards the south. The shifting nature of palaeo-courses and confluences in the highly tectonic potential zone suggests that the middle-lower basin area has been uplifted and southward tilted around the MFF zone.

Keywords Hydrogeomorphological adjustment · Quaternary geological formations · Morphotectonic indices · Tectonic potential zone · Shifting river course

Introduction

The hydrogeomorphological adjustment of a river course within a basin is significantly controlled by the lithological structures and tectonic influences (Alexander and Leeder 1987; Schumm et al. 2000; Sahu et al. 2010; Roy and Sahu 2015). A river adjusts within the lithological layer through widening and drowning its courses depending on the structural upliftment and subsidence (Holbrook and Schumm 1999; Miller et al. 2012; Whittaker 2012; Rao et al. 2013; Ambili and Narayana 2014). All these adjustments are observed through the analysis of river profiles along the longitudinal (long) and transverse (cross)

dimensions. The nature of tilting within a basin is also reflected by the drainage networks (Cox 1994; Salvany 2004). The reach-wise tectonic potentialities can redirect to predict the possible change in hydrogeomorphological processes and associated transformations in the river pattern (USGS 1997; Roy and Sahu 2015). All these changes and adjustments are reflected in the tectonically highly active regions. The nature of river adjustment and resultant signature identifications are quite difficult in the feeble tectonic regions (Wobus et al. 2006; Kirby and Whipple 2012). Still, the imprints of river adjustment can be demarcated by the nature of palaeo-courses after rigorous investigations.

The Dulung is an important tributary system in the middle course of the Subarnarekha basin. The Dulung basin is situated in the complex morphotectonic set-up in the southwestern fringe of the Bengal Basin (Patel and Sarkar 2010; Dandapat et al. 2020). The upper catchment area of the Dulung basin is situated in the Proterozoic fold belt, fringed by the Chotanagpur foothill fault (CFF) (Adewumi and Anifowose 2017). The middle and lower catchment areas

Responsible Editor: François Roure

✉ Subrata Jana
subrata.vumid@gmail.com

¹ Department of Geography, Belda College, Paschim Medinipur, Belda, India 721424

are situated within the CFF and Medinipur-Farakka fault (MFF) zone, composed of thick alluvial deposits over the Bengal Basin. In the perspective of regional tectonics, this basin is located nearer to the subduction zone of the Indian plate under the Eurasian plate at the rate of about 2–4 mm/year (Goodbred et al. 2003; Mukul et al. 2014). This area is surrounded by the Singhbhum and Purulia (north and south) shear zones in the western part in association with other basement faults and subsurface faults in the eastern part (GSI 2000; Mandal et al. 2015). The negative Bouguer gravity anomaly (BGA) is also experienced in this region (GSI 2000). Since 1964, about twenty earthquakes (3.4–5.9 mB) have taken place within 100-km radius of the study area (GSI 2000; Nath et al. 2014; ET 2020), but any earthquake epicenter is not present within the study area. The depths of those epicenters are varied within 10–40 km from the surface (GSI 2000). Among these twenty earthquakes, seven earthquakes happened in the last 10 years (ET 2020). Very recently, on 8th April 2020, a 4.1-mB intensity earthquake was originated at 10 km depth in Bankura district, which is located only about 85 km north of the basin area (ET 2020). Geologically, this area is composed of various types of rocks and sedimentary lithological formations during Lower Proterozoic to Quaternary periods (GSI 2000).

The elongated Dulung basin is aligned from the north–south to south-east direction. In recent times, the mainstream of Dulung River is the confluence with the Subarnarekha River at Rohini. However, another branch bifurcates from the mainstream of Dulung before the confluence with the Subarnarekha River at Ragra, located in the upstream section of Rohini. Moreover, the other two confluences of Dulung River are observed about 12 km and 32 km downstream section from the present confluence position located near Kulboni and Dantan, respectively. These two courses also remained the mainstream of the Dulung River in the past. In the lower catchment area of the entire Dulung basin, the present river course and the palaeo-courses ensure a parallel flow path in conjunction with the Subarnarekha River. The existence of meander scrolls within the interfluvial area of the Dulung and Subarnarekha River indicates that the Subarnarekha mainstream is gradually migrated towards the right (south) from its earlier courses (Jana 2019). Such adjustment of river courses is indicating the tectonic potentiality and structural control within this region.

Several intensive studies were done in the Dulung basin related to the basin morphometry, geology and rock structures, landform and terrain characteristics, and soil characteristics (Patel and Sarkar 2009, 2010; Bera and Bandyopadhyay 2012; Mondal et al. 2012; Sarkar and Patel 2011, 2012, 2017; Roy et al. 2013; Jana and Paul 2019; Dandapat et al. 2020). However, the earlier studies were accomplished concerning the present (upper) basin area (up to Rohini section), but none of

the works was considered in the entire basin area (up to Dantan section) comprising with the pattern of palaeo-courses and confluence shifting of the Dulung river. Moreover, the role of tectonic influences in hydrogeomorphological evolution and adjustment of river system remained unexplored in this area. Therefore, the present study aims to understand the tectonic influences within the entire Dulung basin coupled with the adjustment of the river system in the distinct hydrogeomorphological and lithological ambience.

Materials and methods

Study area

The present study area of Dulung basin is extended between the 21° 54' 35.65" N to 22° 39' 06.10" N and 86° 38' 55.37" E to 87° 16' 52.72" E coordinates and covering an area of 1483.52 km² (Fig. 1). The Dulung basin is situated within the interfluvial region of the river Subarnarekha in the south and Kansai in the north, which confluence with the Subarnarekha River (Fig. 1a).

The north-west to south-east align elongated basin is placed within 9–417-m elevation (Fig. 1b). The northwestern part of the basin is highly elevated and it gradually reduced towards the southeastern part. Geologically, two major faults are found across the basin area, i.e., the CFF in the northwestern part and MFF in the southeastern part (Fig. 1a). Thick alluvium (up to 2100 m depth) was deposited within these two fault zones over the basement of the Bengal Basin. The basin area was formed by different types of hard and soft rocks deposited during the Lower Proterozoic to Quaternary periods (Fig. 2). Most of the basin area is covered by the garnetiferous phyllite of Singhbhum group, the Tertiary gravel bed of Dhalbhum, laterite of Lalgah formation, clay with caliche nodules of Sijua formation, and fine sand-silt-clay of Panskura formation. Most of the lower order streams (mainly 1st and 2nd order) remain in the elevated as well as garnetiferous phyllite and laterite dominated area, whereas the trunk stream with its valley persists in the Sijua surface.

At present, three sub-basins (upper, middle, and lower) exist within the entire selected areas (Fig. 1b). However, the river planform and orientation of the palaeo-courses indicates that it was a single basin in the past. The natural landscape in the lower part of the basin has been intensively modified by anthropogenic activities like settlement constructions over the relatively elevated levee positions, and most of the palaeo-courses are transformed into agricultural land. Despite anthropogenic modifications, the palaeo-courses can be identified from the satellite imageries coupled with on-field observations.

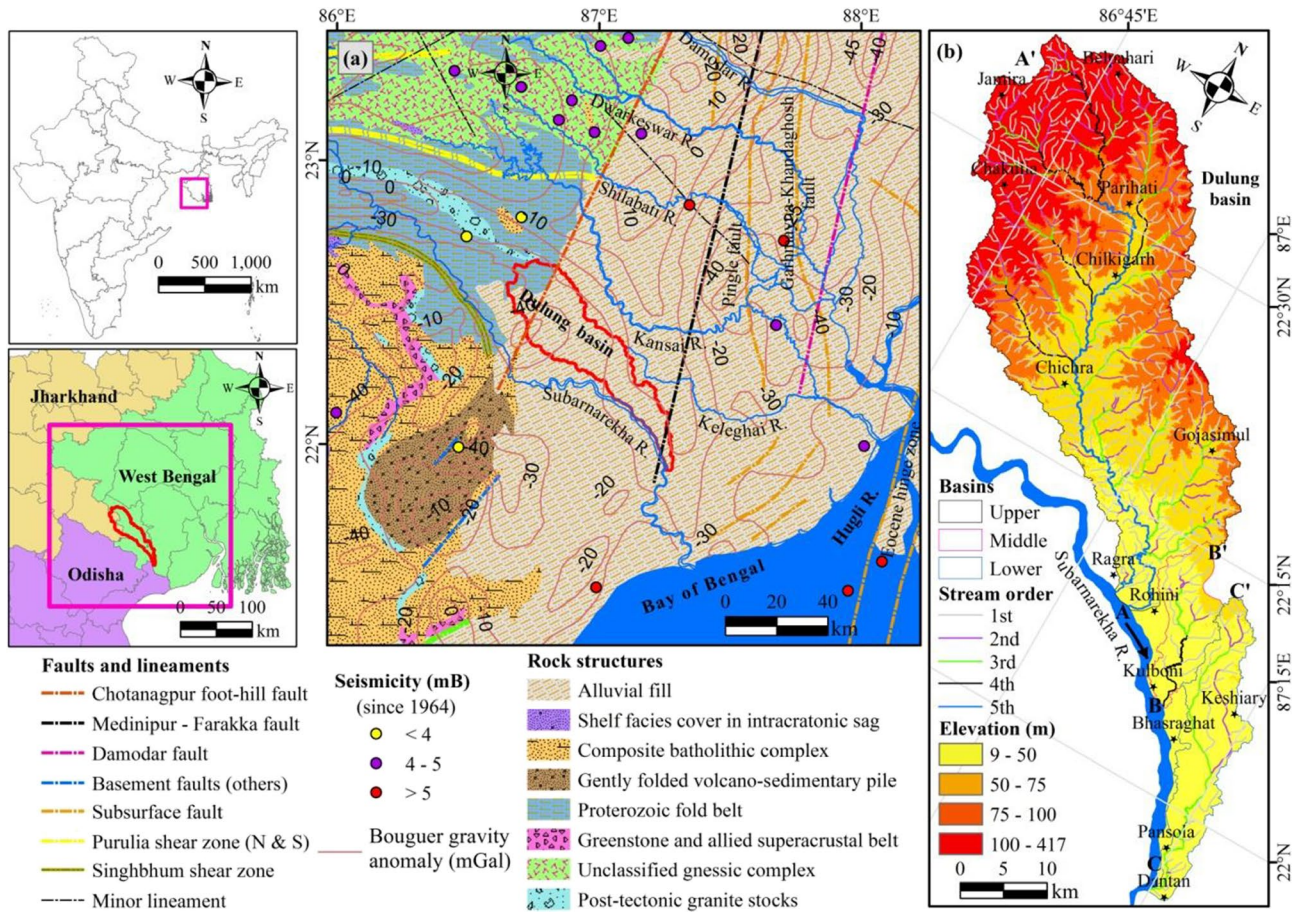


Fig. 1 Location map of the study area shows (a) the tectonic and geological framework in and around the study area in the southwestern fringe of Bengal basin (modified after Seismotectonic Atlas of India; GSI 2000), (b) the existing drainage pattern and stream orders of the

Dulung river system superimposed over the digital elevation map indicating the three main trunk streams AA', BB', and CC' of the upper, middle, and lower basins, respectively

Tectonics and geology

The information about lithological formations of the study area (Fig. 2) has been taken from the Geological Quadrangle Map (sheet number 73-J, N and O) (GSI 1998). The tectonic frameworks (Fig. 1a) of basement depth, rock structures, major faults and lineaments, BGA, and seismicity have been assessed for the study area and its surrounding region based on the Seismotectonic Atlas of India and its Environs (sheet number 23 and 24) (GSI 2000). In the case of basement depth assessment, the area above the 0 m basement contour is considered the negative depth, which indicates the exposure of the parent rock strata (GSI 2000). The inverse distance weighting (IDW) interpolation method (with 10 m cell size) (Philip and Watson 1982) has been adopted with the extracted contours of basement depth and BGA.

Hydrogeomorphological analysis

The hydrogeomorphological analysis has been done to understand the degree of tectonic influence and structural settings over the different segments of the basin. In this aspect, the elevation data has been extracted from the Shuttle Radar Topography Mission (SRTM) 1-arc second (30 m) resolution images coupled with collected elevation data based on differential global positioning systems (DGPS), total station (TS), and auto-level (AL) survey at the different positions of the basin and river cross-sections. The DGPS, TS, and AL surveys were conducted during March–May 2016. The DGPS-based elevation data were randomly taken from 2115 ground points in the different landform segments of the basin. The TS survey was conducted at ten distinct landform areas in the middle-lower section of the basin. About 900–1000 points of elevation data were taken from each site with ~10-m spatial interval depending on

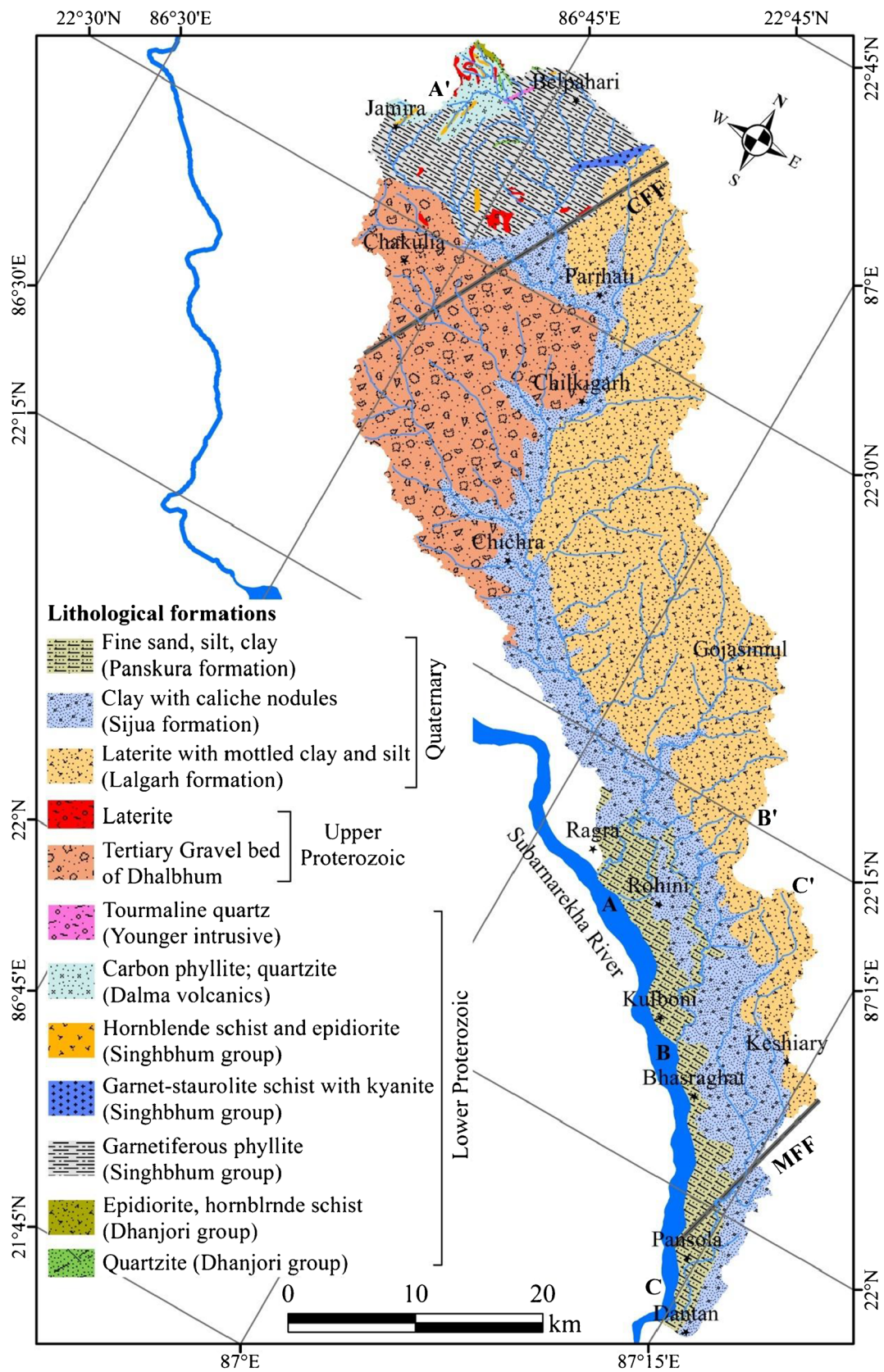


Fig. 2 Age-wise different lithological formations of the study area. AA', BB', and CC' are the main three trunk streams of the study area

the terrain condition. The AL survey was conducted across the trunk stream at fifteen different sites in the lower, middle, and upper basin areas. The 30-m resolution SRTM image has been resampled into 10-m spatial resolution after sub-pixel analysis (Mokarrama and Hojati 2018). The vertical accuracy of the resampled SRTM data has been validated with the DGPS-based elevations, which confers ± 0.12 m of root mean square error (RMSE). The DGPS, TS, and AL survey-based elevation data have been converted into 10-m resolution raster data using the IDW interpolation method (Patel et al. 2016). The survey-based raster data has been fused with the resampled SRTM data to prepare the final 10 m resolution digital elevation model (DEM). Moreover, the different micro-geomorphological features like the natural levee, floodplain, palaeo-course, meander scrolls, and recent river courses have been identified after the field observations, measurements of the topographic conditions, land plot by plot elevation difference, pattern and shape of the combined plots in association with cadastral maps. Alongside the field investigations, the Google Earth (GE) image has been applied to extract the micro-geomorphological features for mapping purposes. The drainage networks and other elevation data have been extracted from the finally primed DEM. Moreover, the extracted drainage networks have been validated and somewhat modified using the GE image. The Landsat 8 satellite image of 28th March 2020 has also been applied to the study of the different landforms as well as to extract the structural lineaments.

Morphometric analysis

The basin-wise morphometric parameters, i.e., stream order (Strahler 1964), bifurcation ratio (R_b), average bifurcation ratio (\bar{R}_b), sinuosity index of the trunk stream (SI), basin perimeter (P), basin area (A), and basin length (L_b) are estimated using the geospatial techniques. Especially, the R_b is estimated as the ratio of the number of streams in an order to the number of streams in the next higher order (Horton 1945). The basin circularity ratio (R_c) is estimated as per Eq. (1) proposed by Miller (1953). Also, the basin form factor (R_f) is computed using Eq. (2) followed by Horton (1932), whereas, the elongation ratio (R_e) is estimated as per Eq. (3) according to the proposition of Schumm (1956).

$$R_c = 4\pi \frac{A}{P^2}. \quad (1)$$

$$R_f = \frac{A}{L_b^2}. \quad (2)$$

$$R_e = \sqrt[3]{\frac{A/\pi}{L_b}}. \quad (3)$$

Isobase and hydraulic gradient

The impacts of tectonic activities and structural influences are observed in the abrupt changes of terrain characteristics and erosional signatures along the river course and mainly in the confluence positions (Keller and Pinter 1996; Silva et al. 2003; Jacques et al. 2014; Kale et al. 2014). In general, the elevations of the confluence positions of the 1st- and 2nd-order streams are considered for isobase analysis (Golts and Rosenthal, 1993; Roy and Sahu 2015). However, in this study, the elevations of all confluence positions have been taken into account for isobase analysis as the 1st- and 2nd-order streams also remained in the lower reaches of the basin.

The hydraulic gradient (HG) has been estimated along the entire drainage network to understand the hydraulic behaviour in the different areas of the basin. The entire drainage system has been considered despite the consideration of only the 1st- and 2nd-order streams (Grohmann 2004; Roy and Sahu 2015), as it does for the isobase analysis. In this case, the 3rd and higher-order streams (having > 5 km length) have been segmented in ~2 km reach length (along the channel) to understand the micro-level variations in hydraulic behaviour under the tectonic influence and lithological diversities. Each of the stream segments has been converted into a pair of points at the upstream and downstream sections to estimate the HG. Elevation of these points is extracted from the DEM. The length of every stream segment is calculated in the ArcGIS 10.4 software. Also, a point is assigned at the middle of each stream segment. The HG of each stream segment has been estimated based on the extracted elevation and stream length using Eq. (4), and the calculated values are assigned in the midpoints of the particular stream segments.

$$HG = \frac{h_c - h_f}{d} \times 100. \quad (4)$$

where h_c is the elevation at upstream/source, h_f is the elevation at downstream/confluence of a stream segment, and d is the length between these two points. The computed results of isobase and HG are assigned at the respective midpoints and interpolated with 10-m spatial resolution using the IDW method in the ArcGIS 10.4 software.

Analysis of morphotectonic and structural variables

Lineament density

The structural lineaments indicate the morphotectonic adjustments of drainage networks in association with the underlying lithological structures (Jacques et al. 2014; NRSC 2014). The lineaments have been extracted from the Landsat 8 image using the Lineament extraction tool in the Geomatica software (Marghany and Hashim 2010; Mwaniki et al. 2015).

Also, the tectonic or major fault guided lineaments have been taken from the geological quadrangle maps of the selected area (GSI 1998). The positions and orientations of the lineaments have been validated with the Landsat 8 and GE images coupled with on-field observations. The extracted lineaments of the marginal parts of the recent and palaeo-courses of the Subarnarekha River have been obliterated during validation. The lineament density (m/m^2) has been estimated considering the 10-m cell size using the Kernel density function in the ArcGIS 10.4 software (Calligaris et al. 2017).

Flow turn angle and regional sinuosity

The zone-wise influences of tectonic activities can be understood from the abrupt change in flow turn angle (FTA) of the streams (Roy and Sahu 2015). The FTA has been extracted from the segmented drainage networks, used for the estimation of HG of the entire basin area. The linear directional mean tool of ArcGIS is used in the estimation of the FTA (compass angle) of each segmented stream (Jozi et al. 2017). Moreover, the estimation of sinuosity index (SI) is an imperative aspect to understand the nature of hydrogeomorphological evolution in the different basin areas (Lindenschmidt and Long 2013). A significant level of changes in river flow patterns can be experienced after tectonic activities (Schumm 1981; Roy and Sahu 2015). The SI is estimated for every stream segment, considering the ratio of actual channel length to the straight line distance (Leopold et al. 1964). The estimated compass angles and SI values have been assigned in the midpoints (same as the midpoint positions used in the HG) of each channel segment and interpolated after the IDW method (with 10 m cell size) to develop the respective raster layers.

Palaeo-channel density

The palaeo-courses are formed due to the migration of active channels into a new course after departing the earlier course. The existence of palaeo-courses in a basin area signifies the impact of morphotectonic processes coupled with the lithostratigraphic association. The palaeo-channel courses have been identified from the GE and Landsat 8 images coupled with DEM and on-field observations. Most of the palaeo-courses have been converted into agricultural land. However, the shape, size, and curvature of the agricultural fields and elevation differences from one to other fields are sharply indicating the planform of the palaeo-courses. The palaeo-courses have been noticed significantly in the middle-lower and lower areas of the Dulung basin, whereas it is meagerly observed in the middle areas and absent in the upper areas of the basin. Therefore, the vector layer of palaeo-courses has been extracted from the middle-lower and lower basin areas using the ArcGIS base map image.

Considering the extracted vector layers, the palaeo-channel density (PC-density) has been estimated using the Kernel density function with 10-m output cell size.

River profiles

The analysis of the long and cross-profiles of a river is an imperative aspect to realize the tectonic influence within a basin (Sharma 1979). The long profiles (AA', BB', and CC') are delineated along the trunk streams of the three distinct basins (Fig. 1b). Elevation data have been extracted from the DEM at every 100-m upstream reach distance accompanying the thalweg positions of the trunk streams. The AL survey was conducted at 15 different positions (meandering and straight course) of the channel cross-sections to estimate the width-depth (w/d) ratio. The elevation data were collected at ~1–5-m intervals across the channel depending on the morphological differences. The database of maximum depth (from the local surface) and channel width have been utilized from the cross-profile data for the estimation of the w/d ratio.

Stream length-gradient index

The stream length-gradient index (SL-index) is an important parameter to assess the presence of active tectonics and morphometric anomalies along the long profile of a drainage network within a basin (Antón et al. 2014; Luirei et al. 2015; Guha and Patel 2017). The SL-index highlights the power of a stream and its magnitude of erosion per unit area with due effects from tectonics, lithological, and fluvial control (Keller and Pinter 1996, 2002; Dar et al. 2014). The SL-index has been calculated by Eq. (5) after Keller and Pinter (2002).

$$SL = \frac{\Delta H}{\Delta L} \times L. \quad (5)$$

where ΔH is the differences of maximum and minimum elevation within a channel reach, ΔL is the length of this reach, and L is the total channel length from the midpoint of the reach (where the index is calculated) in the upstream direction to the water divide (highest point of the channel).

The SL-index can be calculated considering the total length of the channel segments and expected a better result (Etchebehere et al. 2004; Moussi et al. 2018). The SL-index is modified as relation declivity extension index (RDE-index) to represent the relation between the stream energy and slope in each position of a stream (Etchebehere et al. 2004). The RDE-index for a particular stretch of the stream network has been estimated by the same equation (Eq. (4)) (Etchebehere et al. 2006). However, L represents the total length from the lower end to the source of the stream segment instead of length from the midpoint to the source. In this study, the RDE-index has been estimated in ArcGIS 10.4 software using the Knickpoint finder tool (Moussi et al. 2018)

collected from the web-platform (<http://www.neotectonica.ufpr.br/2013/index.php/aplicativos>). The same segmented streams and midpoints (used in HG estimation) have also been utilized for RDE-index estimation. The segmented streams and DEM have been employed for auto-extractions of knick points and RDE-index values of each stream segment. The estimated RDE-index values have been placed at the corresponding midpoints of the stream segments and interpolated in the IDW method with a 10-m cell size.

Analysis of basin inclination under tectonic and structural influences

Transverse topographic symmetry factor

The transverse topographic symmetry factor (TTSF) or T-index represents the deviation of the trunk stream from the basin midline (Roy and Sahu 2015, 2016). Therefore, T-index is a significant indicator to assess the topographic symmetry or asymmetry nature at different reaches of a basin. The T-index value varies from 0 to 1, which represents the absolute symmetry (0) and absolute asymmetry (1). The value comprised between 0 and 1 at the different reaches of a basin suggests an asymmetry in nature (Cox 1994). The T-index is estimated at the different reaches of the trunk stream to assess the degree of tilting and associated tectonic influence within the entire basin as well as at the different reaches of the basin (Sboras et al. 2010; Jacques et al. 2014). In this study, the T-index has been estimated along the three main trunk streams of upper, middle and lower basins coupled with along the other thirteen main tributaries of the upper basin followed by Eq. (6).

$$T = \frac{D_a}{D_b} \quad (6)$$

where D_a is the distance of trunk stream/main tributary from the corresponding basin midline and D_b is the distance of the basin boundary (right side) from the basin midline. Both the distances have been measured at the exact perpendicular to the basin midline. The perpendicular lines have been extracted with the help of the DSAS tool in ArcGIS 10.4 software at 100-m intervals. The estimated T-index values have been pointed at the corresponding positions of the streams and interpolated in the IDW method (with 10 m cell size) to prepare a raster data set.

Drainage basin asymmetry factor

Drainage basin asymmetry factor (AF-index) indicates the nature of tilting (left or right-ward) of a basin in compared the orientations of the trunk stream caused by tectonic activities (Hare and Gardner 1985; Cox 1994; Sboras et al. 2010;

Kale et al. 2014; Siddiqui 2014). The AF-index has been estimated for all three basins as per Eq. (7).

$$AF = \frac{A_r}{A_t} \times 100. \quad (7)$$

where A_r is the basin area of the right side of the mainstream and A_t denotes the total basin area. The value of the AF-index close to 50 indicates the level or slight tilting nature of a basin (Cox 1994). The deviation (above or below) from 50 reveals the tilting of a basin. The tilting maximizes with the value tend towards 100 or 0, which suggests a high magnitude of tilting as a result of active tectonics and associated lithological control (Cox 1994).

Estimation of tectonic potentiality index

The tectonic potentiality index (TPI) has been estimated considering the ten variables (output layers) of basement depth (a), BGA (b), isobase (c), HG (d), lineament density (e), FTA (f), SI (g), palaeo-channel density (h), T-index (i), and RDE-index (j) (Table 1). The database of digital number (DN) has been extracted from every pixel (with 100 m² area) corresponding to each layer. The four categorical rating scores have been assigned as 1, 2, 3, and 4 respectively for low, moderate, high and very high tectonic potential classes depending on the corresponding DN values of every pixel in each layer and its quartile deviations (Table 1). Therefore, ten different categorical rating scores are designated against each pixel. The pixel-wise TPI has been estimated based on Eq. (8) after considering the scores of the ten output layers (Jana 2020).

$$TPI = \sqrt{\frac{a \times b \times c \times d \times e \times f \times g \times h \times i \times j}{10}} \quad (8)$$

The pixel-wise initial estimated TPI values have been modified by the normalization process based on Eq. (9) to obtain the final TPI values (Jana 2020).

$$TPI = \frac{X - X_{\min}}{X_{\max}} \quad (9)$$

where X is the individual TPI value of every pixel, and X_{\max} and X_{\min} are the maximum and minimum TPI value, respectively, among all TPI values (as per Eq. (8)). The pixel-wise estimated final TPI values have been interpolated in the IDW method with 10 m cell size. The low, moderate, high, and very high tectonic potential zones have been demarcated as per the quartile deviations of final TPI values of all pixels. Moreover, the interpolated raster datasets of basement depth, BGA, isobase, HG, lineament density, FTA, SI, PC-density, RDE-index, and T-index have been categorized by four zones in respective maps after considering the quartile deviations of the pixel-based values.

Table 1 Based on the quartile deviations of pixel values of ten variables, the categorical rating scores for estimation of tectonic potentiality index (TPI)

Variables	Categorical rating scores			
	Low (1)	Moderate (2)	High (3)	Very high (4)
Basement depth (m)	< 0	0 to 200	200–500	> 500
Bouguer gravity anomaly (mGal)	< -30	-30 to -25	-25 to -15	> -15
Isobase (m)	< 40	40–70	70–90	> 90
Hydraulic gradient	< 450	450–725	725–950	> 950
Lineament density (m/m ²)	< 0.11	0.11–0.20	0.20–0.27	> 0.27
Flow turn angle (degree)	< 71.28	71.28–93.14	93.14–117.12	> 117.12
Sinuosity index	< 1.04	1.04–1.07	1.07–1.15	> 1.15
Palaeo-channel density (m/m ²)	< 110.14	110.14–235.16	235.16–404.83	> 404.83
Transverse topographic symmetry factor	< 0.22	0.22–0.30	0.30–0.45	> 0.45
Relation declivity extension (RDE-index)	< 12.18	12.18–14.68	14.68–18.42	> 18.42

Results

Variations of Bouguer gravity anomaly and basement depths

The BGA reveals a negative anomaly (–10 to –45 mGal) within the study area (Fig. 3b). The higher BGA (–15 to –10 mGal) is observed in the lower part of the basin, which is gradually decreasing towards the upper basin areas and reaching up to –45 mGal (Fig. 3b). Within the study area, the basement depth of the Bengal Basin varies within 0–2100 m (Fig. 3a), and a similar thick volume of alluvium was deposited over the basement (Fig. 1a). Within the Dulung basin, the higher depth (500–2100 m) is observed in the lower basin areas, which is gradually decreased towards the upper basin areas (up to 0 m limit). The negative depth (–250–0 m) is observed in the upper part of the basin due to the exposure of the rocky surface of the Proterozoic fold belt (Fig. 1a) dominated by garnetiferous phyllite in association with other rocks of the lower Proterozoic period (Fig. 2). The transitional part (0 m) of the basement depth (Fig. 3a) is found along the CFF (Fig. 1a). Tertiary gravel bed of the upper Proterozoic period (Fig. 3) is observed on the right side of the trunk stream in the upper part of the basin (Fig. 1b). The trunk stream follows the surface of the Sijua formation, which is composed of clay with caliche nodules. The basin areas in the left side of the trunk stream remain under Lalgah formation in the compilation of laterite with mottled clay and silt. The areas of meander scrolls of the Subarnarekha River and the palaeo-channels of the Dulung River persist in the surface of Panskura formation composed of fine sand, silt, and clay (Fig. 3).

Geomorphological adjustments

Morphometric diversity

The morphometric attributes of the different basins as well as within the overall basin area have been estimated

(Table 2) based on the empirical formulas. The stream order varies up to the 5th, 4th, and 3rd order in the upper, middle and lower basins, respectively (Fig. 1b; Table 2). The basin-wise perimeter (P) and length (L_b) have been measured, which is mentioned in Table 2. The estimated basin area (A) of the upper, middle, and lower basins are 1190.72 km², 91.81 km², and 161.70 km², respectively, whereas the overall area of the Dulung basin is 1483.52 km². The order-wise number of the stream has been varied according to the variations in basin area and perimeter (Table 2). The resulted R_b of the upper, middle, and lower basins are respectively 4.75, 2.77 and 5.30, whereas it is 4.90 for the overall basin area (Table 2). The estimated SI values of the trunk streams of the upper (AA'), middle (BB'), and lower (CC') basins (Fig. 1b) are 1.54, 1.73, and 1.34, respectively. The basin-wise estimated values of R_c , R_f , and R_e have been varied according to A , P , and L_b (Table 2).

Variation of isobase

The isobase map of the Dulung basin (Fig. 4a) sharply indicates the adjustment of the base level of erosion of the lower-order streams with the higher-order streams. The deformation in the elevation differences at the confluence positions of different streams reveals the erosive nature of distinctive rocks and lithological units. The areas covered by the more resistive Proterozoic rocks and Quaternary laterite (Fig. 2) remain as higher elevated areas with > 70 m of isobase values (Fig. 4a). The isobase zones are nearly matched with the elevation classes (Fig. 1b). However, the crenulated forms have been observed in the elevation classes due to the head-ward erosion of the streams in the form of rills and gullies over the corresponding lithological formations. The CFF align almost parallel to the 90 m isobase value. The below 90 m or specifically below 70 m isobase zones covers the major portion of the basin area (Fig. 4a), which indicates the fall of the local base level of erosion at a certain extent after the CFF with due effects from tectonic action and structural adjustment.

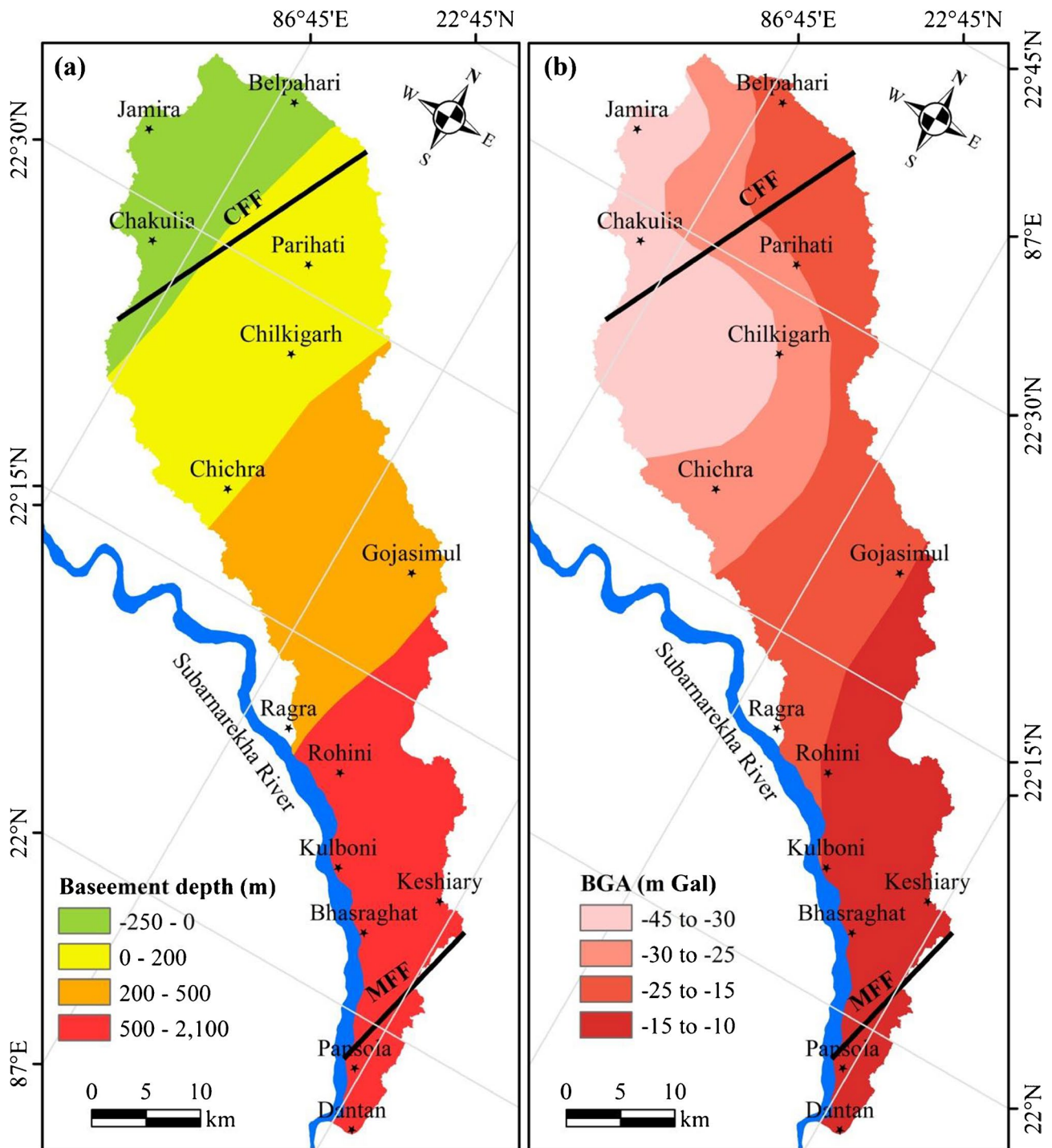


Fig. 3 The simulated (a) basement depth of the Bengal Basin and (b) nature of Bouguer gravity anomaly (BGA) within the study area

Variation of hydraulic gradient

The HG represents the hydraulic behaviour under the tectonic influence and lithological diversities. The areas with higher HG (> 725) are observed in an erratic form in the upper and middle zone of the basin area (Fig. 4b) over the relatively

resistive rock structures (Fig. 2). It is very fascinating that around the MFF the higher HG is also found in the lower basin area (Fig. 4b) where the elevation is low (< 50 m) in comparison to the other higher HG areas of the upper and middle zones of the basin (Fig. 1b). The area of low HG (< 450) is mainly associated with the areas of low elevation and relatively

Table 2 Morphometric attributes of the Dulung River system

Drainage basins	Stream order	Stream number	Total stream length (km)	(R_b)	$(\overline{R_b})$	Other parameters
Upper	1 st	509	739.07	4.75		$P : 226.35 \text{ km}; A : 1190.72 \text{ km}^2; L_b : 66.79 \text{ km}; SI : 1.54; R_c : 0.29; R_f : 0.27; R_e : 0.58$
	2 nd	106	237.31	4.80		
	3 rd	23	158.17	4.61		
	4 th	5	70.48	4.60		
	5 th	1	82.80	5.00		
Middle	1 st	19	48.77	2.77		$P : 62.37 \text{ km}; A : 91.81 \text{ km}^2; L_b : 19.60 \text{ km}; SI : 1.73; R_c : 0.30; R_f : 0.24; R_e : 0.55$
	2 nd	5	8.51	3.80		
	3 rd	2	10.98	2.50		
	4 th	1	15.94	2.00		
Lower	1 st	28	55.44	5.30		$P : 110.41 \text{ km}; A : 161.70 \text{ km}^2; L_b : 35.82 \text{ km}; SI : 1.34; R_c : 0.17; R_f : 0.13; R_e : 0.40$
	2 nd	5	21.73	5.60		
	3 rd	1	39.74	5.00		
Overall	1 st	556	843.27	4.90		$P : 310.70 \text{ km}; A : 1483.52 \text{ km}^2; L_b : 100.28 \text{ km}; R_c : 0.19; R_f : 0.15; R_e : 0.43$
	2 nd	116	267.55	4.79		
	3 rd	26	208.88	4.46		
	4 th	6	86.42	4.33		
	5 th	1	82.80	6.00		

Bifurcation ratio (R_b), average bifurcation ratio ($\overline{R_b}$), sinuosity index of the trunk stream (SI), basin perimeter (P), basin area (A), basin length (L_b), basin circularity ratio (R_c), basin form factor (R_f), and basin elongation ratio (R_e).

soft sedimentary lithological structures. However, the low and moderate (450–725) HG is also observed in the higher elevation areas (mainly in the Belpahari–Parihati zone) around the CFF zone (Fig. 1a) of the upper and middle zones of the basin. The zone-wise diversity of HG reveals that alongside the lithological factors, the tectonic deformations also act an important role within the basin areas.

Fluvial adjustments under tectonic and structural control

Lineament density

The high (0.20–0.27 m/m²) to very high (0.27–0.63 m/m²) lineament density is observed in the upper and middle section of the basin area (Fig. 5a). In the upper basin area, the streams have pursued the structural lineaments of the hard and erosion resistive rocks (Fig. 2) in the Proterozoic fold belt. However, the very high lineament density is found under the control of lithological structures in the middle course of the basin. The moderate density (0.11–0.20 m/m²) is obtained mainly in the middle section and the extreme lower section of the basin, whereas, the low density (<0.11 m/m²) is observed in the upper and lower part of the basin.

Flow turn angle and sinuosity index

The FTA varies from 0.06 to 179.88° within the entire basin area (Fig. 5b). Higher FTA (>93.14°) is found mainly in the upper and lower section of the basin and some pockets in the middle section. Lower FTA (0.06–71.28°) is resulted in the patchy form in the entire basin, mainly at the high–moderate elevation areas associated with the relatively steep slope. The moderate FTA (71.28–93.14°) is found adjacent to the low–high FTA within the entire basin depending on the rock structures and elevation differences. The SI differs from 1 to 3.02 within the entire basin area (Fig. 5c). The higher SI (>1.07) is observed along the trunk stream and its main tributaries in the different stretches of the basin. The higher FTA and SI in the upper course are associated with the structural fold belt, CFF zone and deformations of rock structures. The higher FTA and SI are associated with the existence of sedimentary layers in the lower course. The lower SI (<1.04) is found in the upper-middle part of the basin over the gravel bed on the right side of the trunk stream and a relatively steeper laterite layer on the left side of the trunk stream. The moderate SI (1.04–1.07) is observed in the left side of the trunk stream dominated by rills and gullies in the laterite layer in the left side of the trunk stream.

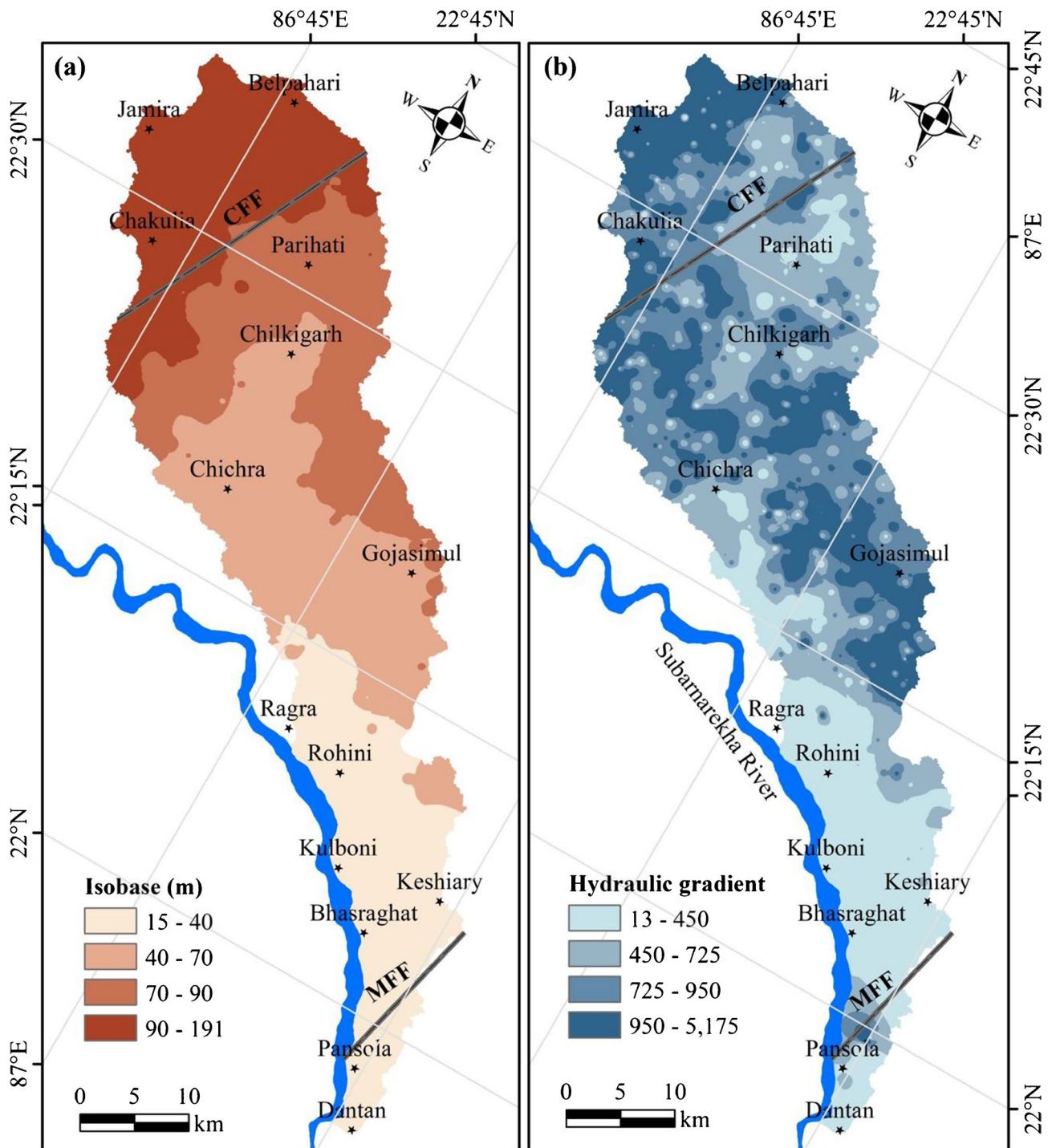


Fig. 4 The variation of (a) isobase and (b) hydraulic gradient (HG) reveals the pattern of hydrogeomorphological configuration of the Dulung basin

Palaeo-channel density

The palaeo-courses of the Dulung River are observed within the concentrated zone of the lower part of the basin (Fig. 5d). The signature of palaeo-course is meagerly present

only in few places besides the trunk stream in the middle part of the basin, and palaeo-courses do not present in the rest of the upper basin area. Therefore, the PC density has been estimated considering the palaeo-courses in the middle-lower and lower parts of the basin. The PC density

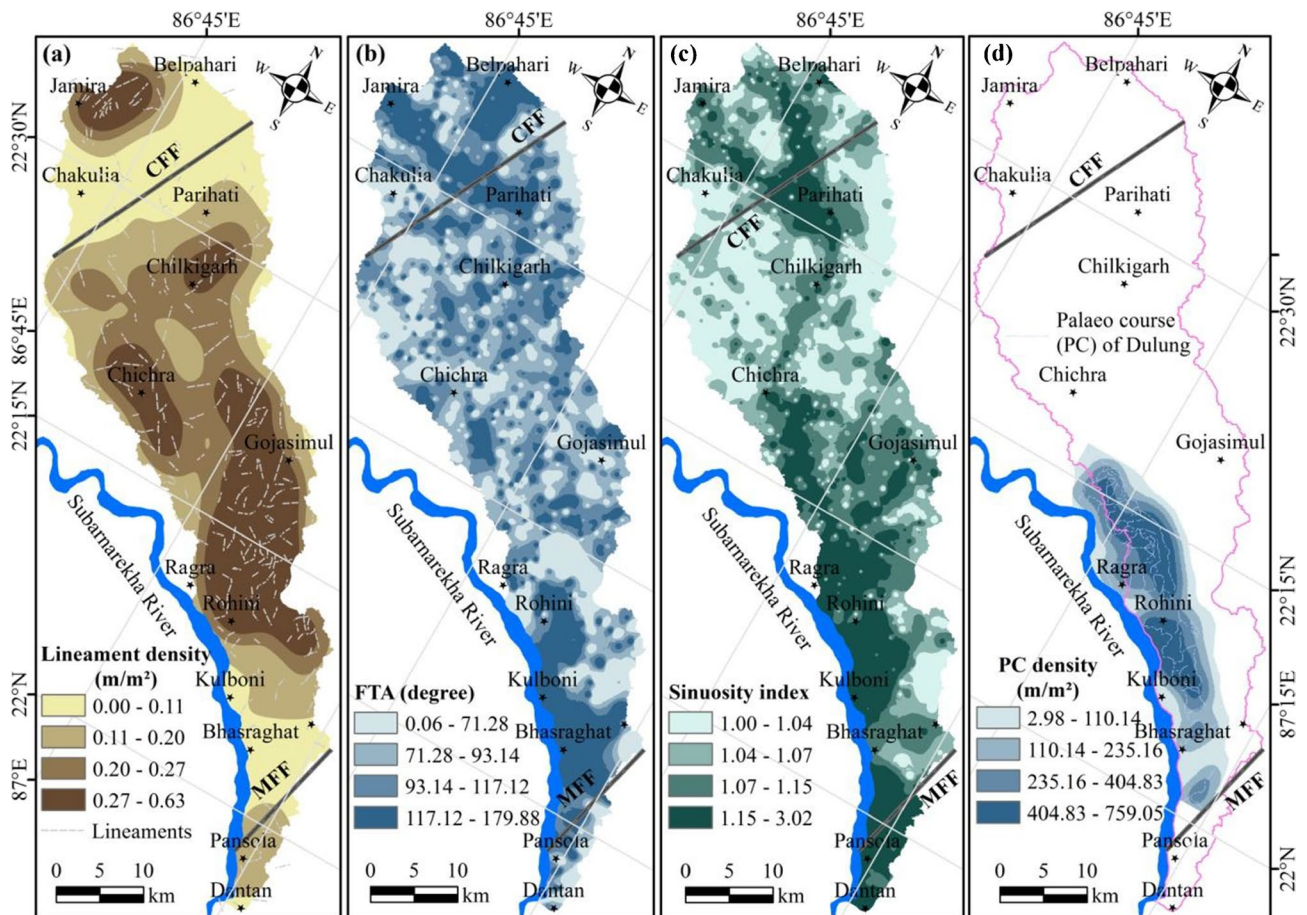


Fig. 5 The adjustment of drainage system under tectonic and structural control was analyzed by (a) lineament density, (b) flow turn angle (FTA), (c) sinuosity index, and (d) palaeo-channel (PC) density within the Dulung basin

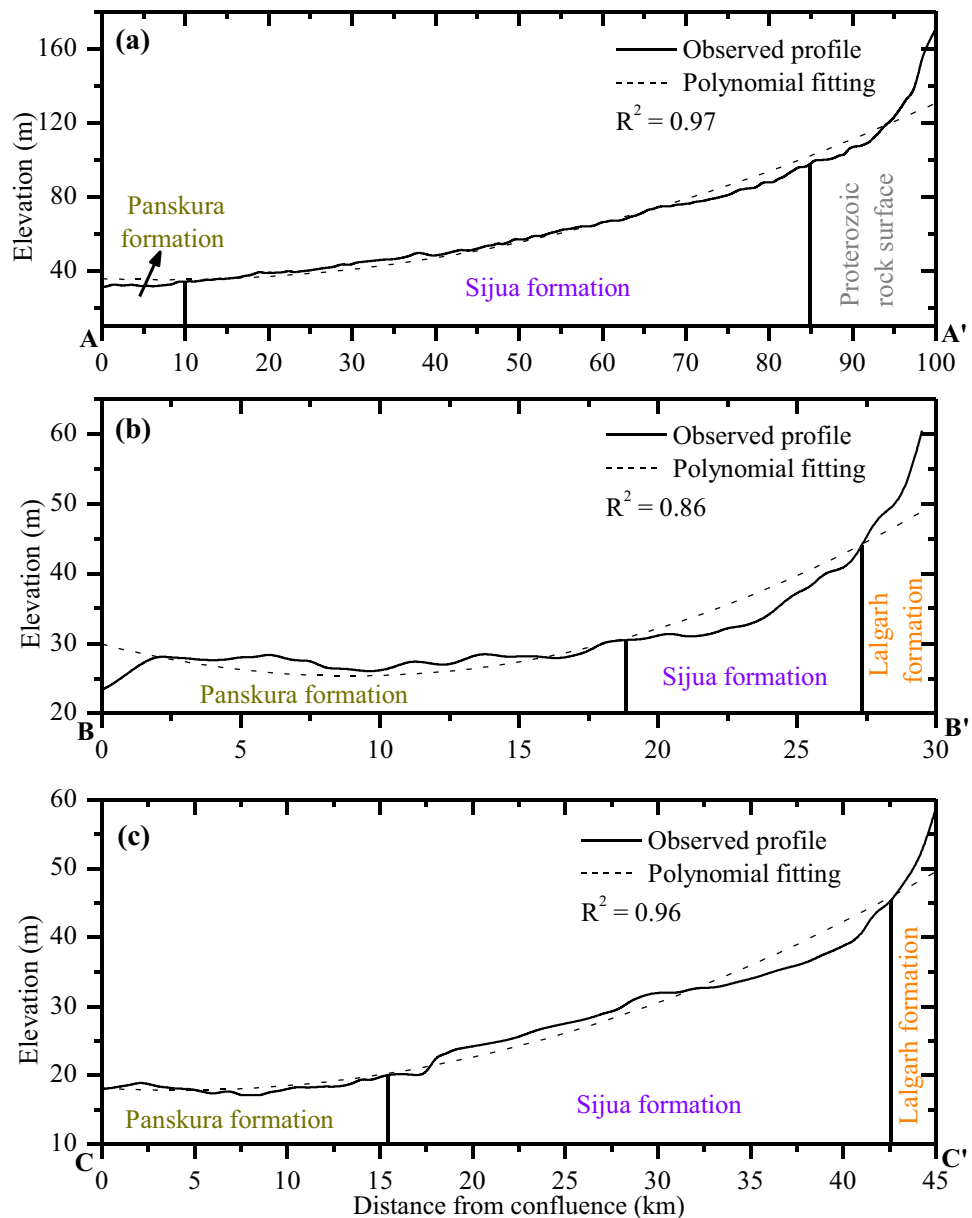
varies from 2.98 to 75,905 m^2/m^2 within the lower part of the basin (Fig. 5d). The PC density has been estimated considering the positions of the palaeo-trunk stream of the Dulung River and their distributaries which were confluence with the mainstream of Subarnarekha River in the past. The PC density map reveals that the low–moderate density class ($< 235.16 \text{ m}^2/\text{m}^2$) is associated with the minimum number of palaeo-courses in the lower part (Fig. 5d) of the lower basin area (Fig. 1b). The higher ($> 235.16 \text{ m}^2/\text{m}^2$) PC density (Fig. 5d) with the maximum number of palaeo-courses is observed in the lower catchment areas of the middle and upper basins (Fig. 1b).

Changes in channel form

The analysis of longitudinal profiles and their changes in the break of slope and elevation coupled with trend lines (second-degree polynomial) along the three trunk streams of the upper (AA'), middle (BB'), and lower (CC') basins (Figs. 1b and 6) suggests the polycyclic evolution of the entire study area. The 100 km long profile of the upper basin

divulges the relatively elevated profile (~9 km stretch, within 91–100-km distance from the confluence) over the hard rock structures (Fig. 2) of the Proterozoic fold belt (Fig. 1a) at the extreme upper section of the basin (Fig. 6a). The elevation of long profile (AA') is reduced within ~24 km stretch (within 67–91-km distance from the confluence) (Fig. 6a) at the transitional zone of the CFF (Fig. 1a). The upper portion of this stretch is also composed of hard rock structures (Fig. 2) of the Proterozoic fold belt (Fig. 1a), whereas, the lower portion is formed by the soft sedimentary layer of Sijua formation (Fig. 2). The middle portion of the profile (within 45–67-km distance from the confluence) is in equilibrium condition and slightly raised within 17–45-km distance from the confluence (Fig. 6a), although, these two sections are formed by the soft sedimentary layers of Sijua formation (Fig. 2). The profile is lowered down at the extreme lower ends of the trunk stream of the upper basin (Fig. 6a) through maintaining the base level of erosion (adjusted to the Subarnarekha River bed) over the fine sand, silt, and clay dominated soft sedimentary layer of Panskura formation (Fig. 2). Similarly, the long profiles of BB' and CC' indicate the polycyclic nature of landform

Fig. 6 Longitudinal profiles over the different lithological formations reveal the river bed elevation along the trunk streams of (a) upper, (b) middle, and (c) lower basins within the Dulung river system. The trunk streams (AA', BB', and CC') are denoted in Figs. 1b and 2



evolution in the lower section of the study area (Fig. 6b, c). The trunk streams of the middle and lower basins are originated (Fig. 1b) from the degraded lateritic uplands of the Lalgarh formation (Fig. 2). The elevated profiles are observed up to the extreme ends of the lateritic uplands and sudden elevation reduction is observed over the sedimentary layers of Sijua formation. The BB' profile is uplifted at the lower section (Fig. 6b) of fine sand, silt, and clay dominated soft sedimentary layer of Panskura formation. Nearer the confluence position, the elevation of the BB' profile is reduced with due effects from the adjustment with the Subarnarekha River through maintaining the base level of erosion. However, the slightly fluctuating condition (up and down) is observed in the CC' profile (Fig. 6c) over the same kind of sedimentary layers of Panskura formation.

The width-depth ratio (w/d) of the trunk streams has been estimated at the fifteen different positions in the lower and middle reaches. All the seven cross-sectional positions of the lower and middle basins (Table 3) are located within the low elevated surface composed of fine sand, silt and clay materials of Panskura formation. In the upper basin (Table 3), only the Dangarsari site is located over the area of Panskura formation, whereas all other sites have been located over the surface of the Sijua formation. The estimated w/d ratio varies within 4.33–71.28 (Table 3). In general, the w/d ratio increases with the increasing distance towards the upstream from the confluence (Rhoads et al. 2009). The overall regression analysis (r) also endorses the strong positive (0.86) relationship between the upstream distance and w/d ratio (Fig. 7). However, the w/d ratio of the upper basin

follows the general rule, whereas the w/d ratio does not follow the general rule in the case of the lower and middle basins (Table 3). In the middle basin, the w/d ratio gradually decreased with the increasing upstream distance from the confluence (Table 3). In the lower basin area, the minimum w/d ratio (4.33) is recorded at the Kunja Baghra site (in the middle stretch of the trunk stream) compared to the downstream and upstream sections (Table 3). The resulting w/d ratio of the upper basin area shows a gradual increase and decrease in the different channel sections (Table 3).

Variation of RDE-index

The RDE-index map represents the relation between the stream energy and slope in each stream segment. The RDE-index varies from 10.00 to 89.53 within the whole basin area (Fig. 8a). The higher stream length-gradient analysis-based RDE-index (> 14.68) is associated along the trunk stream and its main tributaries having the 3rd- and above-stream orders mainly in the upper and middle catchment areas. Also, the higher RDE-index has resulted in the lower catchment areas near the Rohini–Kulboni and Bhasraghat sections. The low RDE-index (< 12.18) is observed mainly in the upper-middle and lower catchment area dominated by laterite soil, as well as soft sedimentary surfaces of the lower catchment area. The low RDE-index zone has been drained by the 1st-order streams mainly on the right side of the trunk stream. However, in the lower catchment area, the low RDE-index is found in the areas drained by the 1st–3rd-order streams. The moderate RDE-index (12.18–14.68) is dominated within the areas of the 1st- and 2nd-order streams.

Tectonic influences on basin (T-index and AF-index)

The influence of tectonic action can be well established through the symmetry or asymmetry factors in the transverse section of the basin (Cox 1994; Perez-Pena et al. 2010). The trunk streams of the three main basins and other main tributaries of the sub-basins of the upper basin (Fig. 1b) are not following the basin middle position. Therefore, the T-index varies from 0.01 to 0.94 (Fig. 8b). The basin asymmetry increases with the higher values of the T-index (Verrios et al. 2004; Toudeshki and Arian 2011). The higher T-index values (> 0.30) have been found in about 60% of areas of the entire basin, which indicates the strong tectonic influence. However, the spatial distribution of the higher T-index is mostly found in the Parihati–Chilkigarh zone (at the lower part CFF zone) of the upper catchment area, and in the major portion of the middle and lower catchment areas. The low T-index values (< 0.22) are mainly found in the upper and middle catchment areas dominated by hard rocks and laterite layers. The AF-index values of the upper, middle, and lower basins are 47.09, 44.24, and 37.62, respectively. The

basin-wise AF-index indicates the asymmetry nature of the Dulung basin. Moreover, the asymmetry nature has gradually increased (with the higher deviations from the AF index of 50) towards the lower basin area.

Tectonic potentiality

The tectonic potential zones have been assessed based on the TPI of the entire study area (Fig. 9a). The very high TPI (> 0.18) and associated high tectonic potential zone is observed in the extreme upper (north-western) part near Jamira and Belpahari area, in the Parihati–Chilkigarh zone, almost the entire middle-lower section of the catchment area (Fig. 9a). The low TPI (< 0.06) is noticed over the hard rock dominated upper catchment areas and in the marginal parts of the lower catchment areas. The moderate–high TPI is found in an erratic form in the different parts of the study area. The confluence positions of the trunk streams remain under the high–very high tectonic potential zones near the Pansola, Kulboni–Bhasraghat, and Ragra–Rohini areas, and the positions are shifted within this highly tectonic potential stretch (Pansola–Ragra) of the lower catchment area.

Discussion

Hydrogeomorphological adjustments under tectonic and structural control

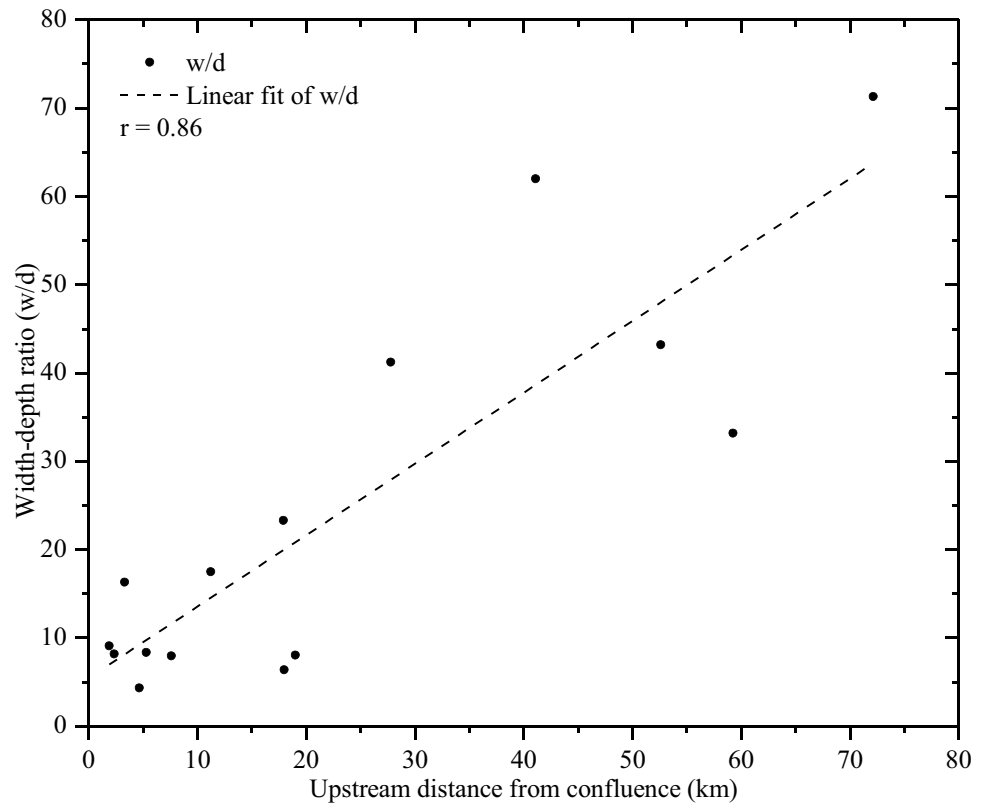
Maximum up to the 5th-order stream has existed over the various lithological settings and elevation differences within the basin area. The 5th-order stream has been originated in the upstream reach just near Parihati (Fig. 1b). The highest stream intensity has been observed in the upper catchment areas over the garnetiferous phyllite surface where the large number of lineaments is observed. The CFF is aligned at the fringe of the phyllite layer. The trunk stream follows the curvature path in the Parihati–Chilkigarh stretch (Fig. 1b) over the soft sedimentary layer of the Sijua formation (Fig. 2) with due effects from deformations in lithological layers nearer to the CFF. At that position, the local base level of erosion has been fallen at below 70 m isobase zone and the river long-profile has lowered down through headward erosion with down cutting action. Such type of river course has been found nearer to the areas of Pora Diha, Dharsa, Gamarra, Nagdi, and Chilkigarh sections, which is also mentioned by Saha et al. (2020). Moreover, the existence of Tertiary gravel bed (on the right side of the trunk stream) persists the trunk stream to follow the curvature path. The trunk stream is flowing (north-west to south-east direction) over the same sedimentary layer in the lower course after maintaining the general slope of the region. However, the trunk stream is sharply turned (near Kubda) towards the south over

Table 3 Site-specific channel cross-sectional dimensions of the corresponding trunk streams of the basin estimated from the field

Basins	Sites	¹ Lat/long at right bank side	¹ Local elevation from MSL (m)	² Upstream distance from confluence (km)	³ Channel width (m)	⁴ Maximum depth (m)	Width-depth ratio (w/d)	Channel pattern and bed form
Lower	Bara Baghra	21° 55' 43.08" N 87° 15' 31.41" E	21.03	2.34	22.52	2.76	8.16	Meander head; pool position at right side
	Kunja Baghra	21° 56' 38.64" N 87° 15' 06.92" E	19.51	4.67	13.59	3.14	4.33	Just downstream position of the meander bend; riffle position
	Rajnagar	22° 01' 14.93" N 87° 13' 41.78" E	45.42	18.99	23.47	2.92	8.04	Straight course; riffle position
Middle	Kalametya	22° 06' 07.87" N 87° 09' 30.39" E	26.52	1.87	21.03	2.31	9.10	Meander head; pool position at right side
	Pabnia	22° 07' 05.60" N 87° 08' 47.92" E	28.04	5.31	16.12	1.93	8.35	Just downstream position of the meander bend; riffle position
	Beniadiha	22° 07' 38.78" N 87° 08' 50.62" E	27.43	7.61	17.86	2.24	7.97	Just downstream position of the confluence of other channels; riffle position
Upper	Nehar	22° 10' 07.58" N 87° 08' 01.94" E	28.35	17.98	9.69	1.52	6.38	Straight course; riffle position
	Dangarsari	22° 10' 30.37" N 87° 05' 22.88" E	30.78	3.31	60.05	3.68	16.32	Straight course; riffle position
	Bhagabanchak	22° 12' 35.80" N 87° 03' 22.28" E	32.92	11.22	54.56	3.12	17.49	Just upstream position of the meander bend; riffle position
	Shuriam	22° 14' 17.08" N 87° 01' 50.96" E	38.10	17.92	80.47	3.45	23.32	Meander head; pool position at right side; mid-channel bar
	Parshana	22° 16' 13.39" N 86° 58' 34.36" E	43.89	27.79	91.14	2.21	41.24	Just upstream position of the meander bend; riffle position; rocky exposure on bed
	Kodopindra	22° 19' 41.95" N 86° 54' 07.13" E	51.82	41.09	145.69	2.35	62.00	Meander head; pool position at right side; rocky exposure on bed
	Mahisamura	22° 24' 32.42" N 86° 52' 06.41" E	60.35	52.60	93.27	2.16	43.18	Meander head; pool position at right side; just downstream position of the confluence of other channels
Ranisal	22° 27' 29.48" N 86° 52' 54.06" E	65.84	59.25	67.67	2.04	33.17	Meander head; pool position at left side; point bar at right side	
Bhelaitikri	22° 30' 23.33" N 86° 49' 24.82" E	79.86	72.14	132.59	1.86	71.28	Meander head; pool position at right side	

Estimated by the ¹GPS survey, ²Google Earth image, ³measuring tape, and ⁴Dumpy level survey

Fig. 7 The estimated width-depth ratio (w/d) at different reaches of the trunk streams of the Dulung basin showing a strong positive correlation



the sedimentary layer of Panskura formation at the lower ends of the trunk stream, just before the confluence with the Subarnarekha River (near Ragra and Rohini). The course has narrowed down and the hydraulic perimeter adjusted with increasing depth over the soft sedimentary layer; however, the course needs to be wider in the lower course dominated by soft sediments. This is related to channel incision into the older sedimentary layer associated with the strong monsoon flow. Moreover, such type of adjustment might be associated with tectonic action in the very high TPI zone (Fig. 9a) and the surface has been raised around the upper part of the MFF. The higher BGA (-10 mGal) also support the high tectonic potentiality and associated lithological deformations in the lower catchment areas. The prominent elevate or nearly equilibrium condition of the long-profiles in the lower reaches of the trunk streams (Fig. 6) also reveals the raised of the lower catchment areas.

The spatial hydrogeomorphological diversities are associated with the tectonic influence and lithological structures within the basin area. The highly tectonic potential zones are found in the different sections, i.e., near Jamira, Belpahari, Parihati, and Chilkigarh in the upper section, most of the areas in the middle section, and Rohini, Kulboni, Bhasraghat, and Pansola areas in the lower section of the entire basin (Fig. 9a). To some extent, these areas remain with higher lineament density, FTA, SI, and RDE-index (Figs. 5a–c, and 8a). The higher FTA and SI are also

observed around the CFF and MFF zones in the upper and lower sections of the basin. The higher lineament density is observed at the extreme upper section of the basin dominated by carbon phyllite and garnetiferous phyllite, and in the middle-lower section of the basin under the tectonic influence and lithological structures (laterite surface). Moreover, the areas of higher RDE-index also confers that the river courses have adjusted under the tectonic influence, lithological structures coupled with stream energy based on the local base level of erosion.

Adjustment of Dulung basin under tectonic and structural influences

The flow direction is associated with the natural surface gradient coupled with the dip direction of the underlying rock strata (Miller 1991). The tilting nature of the subsurface lithological structures is influenced by the nature of active tectonics (Schumm et al. 2000). The resulted T-index reveals that after the CFF zone, the higher asymmetry (> 0.30) is found within the entire middle and lower basin area (Fig. 8b). In the upper basin, the trunk stream is flowing through the left side of the basin midline only in the upper catchment area up to the Chilkigarh section. Afterwards, the trunk stream is flowing on the right side of the basin midline up to the confluence position. The stream is flowing with high deviation (compared to the basin midline) at the

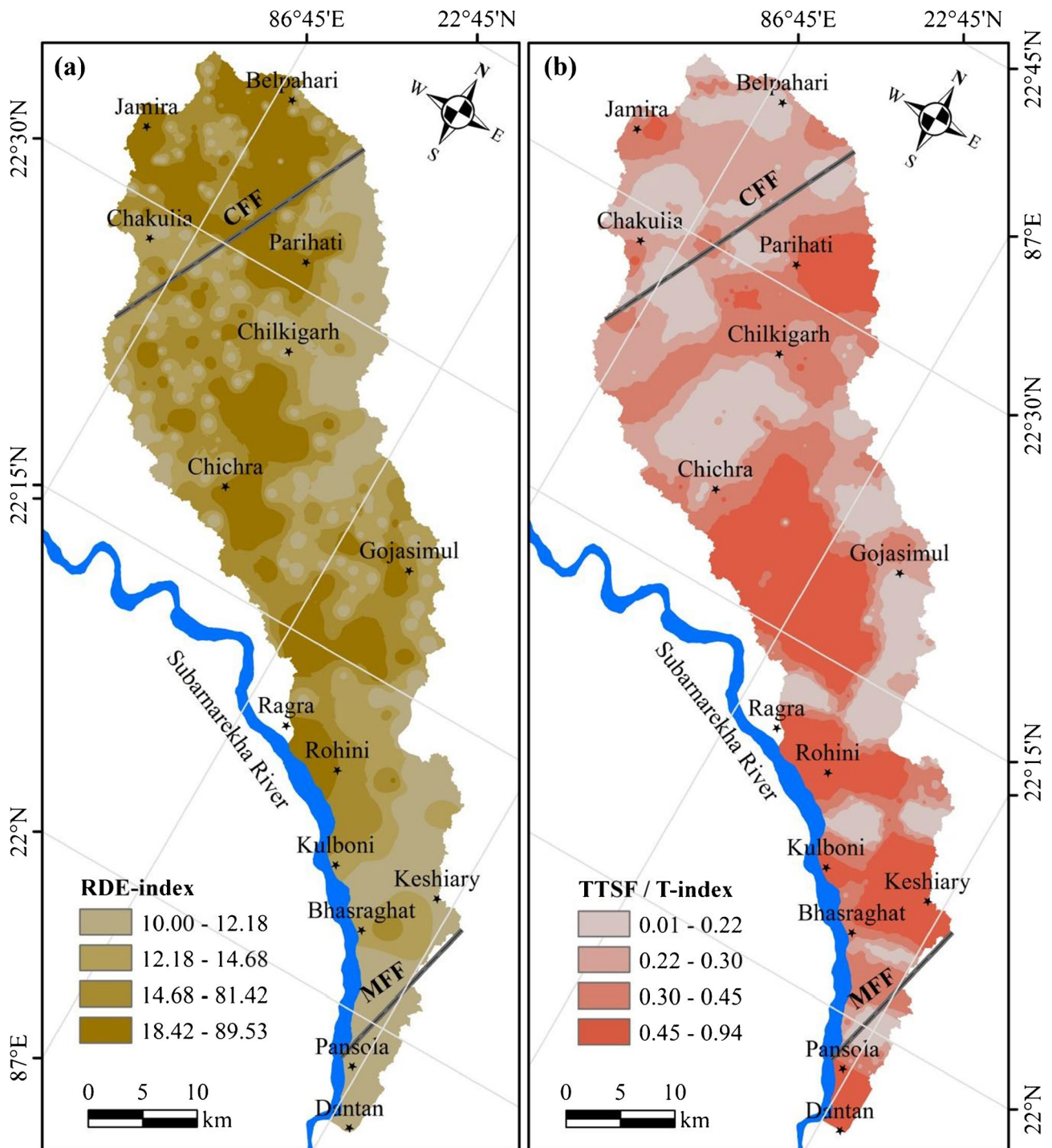


Fig. 8 Spatial variation of tectonic influences within the basin was assessed by the (a) relation declivity extension index (RDE-index) and (b) transverse topographic symmetry factor (TTSF / T-index)

Chichra–Rohini stretch of the upper basin area (Fig. 8b). A similar type of reach-wise asymmetry is observed in the middle and lower basins. The basin-wise AF-index also indicates the tilting nature of the study area. The AF-index values gradually decreased (highly deviated from the

symmetry factor, i.e., 50) towards the lower basin areas, which reveals that the tectonic potentiality and associated lithological deformations have been active in between the CFF–MFF regions. The pattern and positional extent of the meander scrolls also indicate that the Subarnarekha River

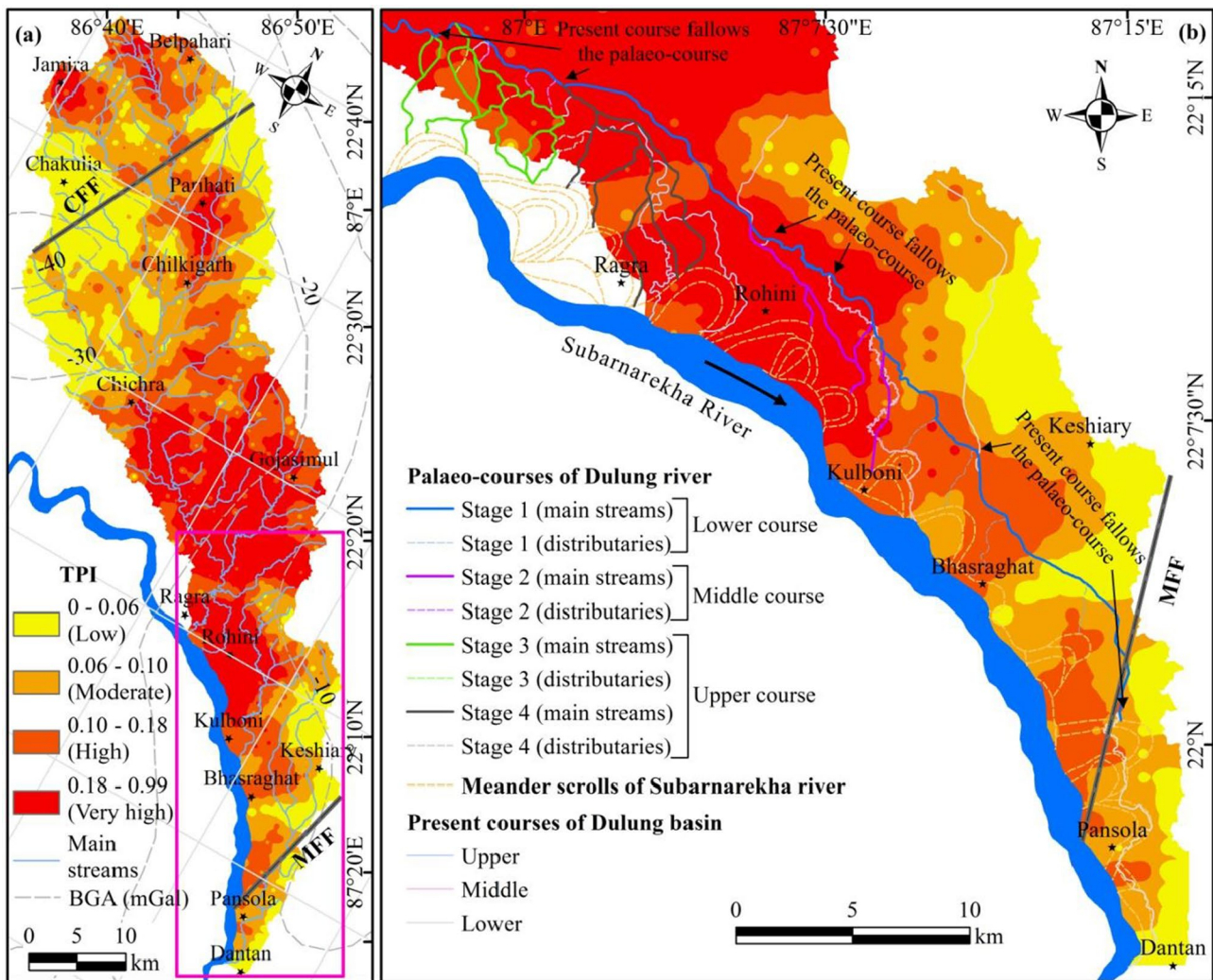


Fig. 9 In the Dulung basin, (a) the tectonic potential index (TPI)-based tectonic potential zones synchronized with the isolines of Bouguer gravity anomaly (BGA), and (b) the present and palaeo-courses adjust through course shifting within the middle-lower area

course gradually migrated towards the right side (south) (Jana 2019) within the study area (Fig. 9b). In the overall analysis of the pattern and orientation of trunk streams and meander scrolls of the Subarnarekha River coupled with T-index and AF-index, it can be concluded that the basin has been tilted in the north to south direction after the CFF zone.

Adjustment of river course under tectonic and structural influences

The trunk streams have adjusted with the tectonic influence and lithological settings in the upper and middle section of the basin area, which is discussed in the earlier section. Now, this section discussed the adjustment of river course in the higher tectonic potential areas of the middle-lower and lower courses of the basin. It is also mentioned that the entire study area is divided into three (upper, middle, and lower)

basins as per the present situation of the drainage networks (Fig. 1b). However, the existence of palaeo-channels reveals that the Dulung River system was extended up to the extreme lower end of the study area before the confluence with the Subarnarekha River near Dantan in the past (Fig. 9b). In this study, the mainstreams and their distributaries of all four stages have been identified through the analysis of relative shape, size, and curvature of the palaeo-courses. The palaeo-courses have been partially survived as low-lying areas, wetlands, water bodies and agricultural lands even after rigorous anthropogenic modifications. The palaeo-channel margin relatively elevated natural levees have been utilized for settlements. However, any dated records have not been used to understand the exact period of positional shifting of the palaeo-courses within this stretch of the basin, as any sediment samples have not been dated either in the present study or any such records have not found from the

previous studies. Therefore, only some relative periods have been mentioned for discussions of the positional shifting of palaeo-courses.

The existing trunk streams and the palaeo-courses of the Dulung River system reveal that to some extent the recent courses of the three basins have been follow the mainstream course of stage 1 (Fig. 9b). Initially (in stage 1), the Dulung River was confluence with the Subarnarekha River in a far upstream position compared to the present confluence position (near Dantan) of the trunk stream of the lower basin (Fig. 9b). In that stage, the Subarnarekha River was flowing ~4 km left side of the present course and the palaeo-course has remained as a meander scroll (Jana 2019). In the lower section, the flow path of the present trunk stream of the lower basin has been directed by the orientation of meander scrolls. In stage 2, the trunk stream of Dulung was confluence about 15 km upstream position (near Kulboni) in compared to stage 1, and the streams of stage 1 have remained as palaeo-channels. However, the present trunk stream of the lower basin has been following the earlier course. The Dulung River was confluence with the Subarnarekha River at the upper course in stage 3 (Fig. 9b) after departing from the main course of stages 1 and 2. In stage 3, a bunch of streams were bifurcated from the mainstream of Dulung after maintaining the local level hydrogeomorphological and lithological adjustments. Finally, in stage 4, the Dulung River was confluence just after the lower section of stage 3 (near Ragra). The present Dulung River has maintained nearly the same course as stage 4. The overall pattern and positional extent of the confluences of the trunk streams of one to another stage reveal that the courses have confluence to the Subarnarekha River with about 12–15-km inter-confluence distance. Such a condition indicates that the upper section of MFF somehow rises at the same rate during

a certain period and the river courses of all stages adjust accordingly. Moreover, the present course has bifurcated in two branches (upper and lower) before the confluence with the Subarnarekha River near Ragra and Rohini (Fig. 9). Recently, the lower branch (near Rohini) is dominated in terms of river dimension and flow energy, however, the upper branch (near Ragra) was the mainstream in the near past (Fig. 9). Also, the recent trunk streams of the middle and lower basin confluences with the Subarnarekha River in far downstream sections from their initial confluence positions. The downward confluence shifting of all the three trunk streams indicates that there might be a relative descend and southward tilting of land in the margin of MFF in recent times. This nature has also been supported by the evidence of the southward shifting of the Subarnarekha River in the studied section and its downstream section (Jana 2019).

The stage-wise relative position of the palaeo-courses within the tectonic potential zone of the middle-lower and lower basin areas reveals that the Subarnarekha River and its tributary (Dulung River) shifts their courses and adjusted under the tectonic influence in the areas of higher BGA and deformed lithological structures. However, the hydrogeomorphological complexities were observed in stream patterns (in stages 3 and 4) and associated landforms in the middle-lower part of the basin. Such types of complexities are associated with the sudden decline of HG (Fig. 4b) and structural deformations supported by the higher level of lineament density, FTA, SI and PC density (Fig. 5). The intricate channel pattern in the middle part of the basin is indicated by the relative positions of palaeo-courses, levees and floodplains, and the avulsion nature of river courses coupled with meander scrolls (Fig. 10). The river courses are progressively shifted towards the newer course (mainly on the southern side) after

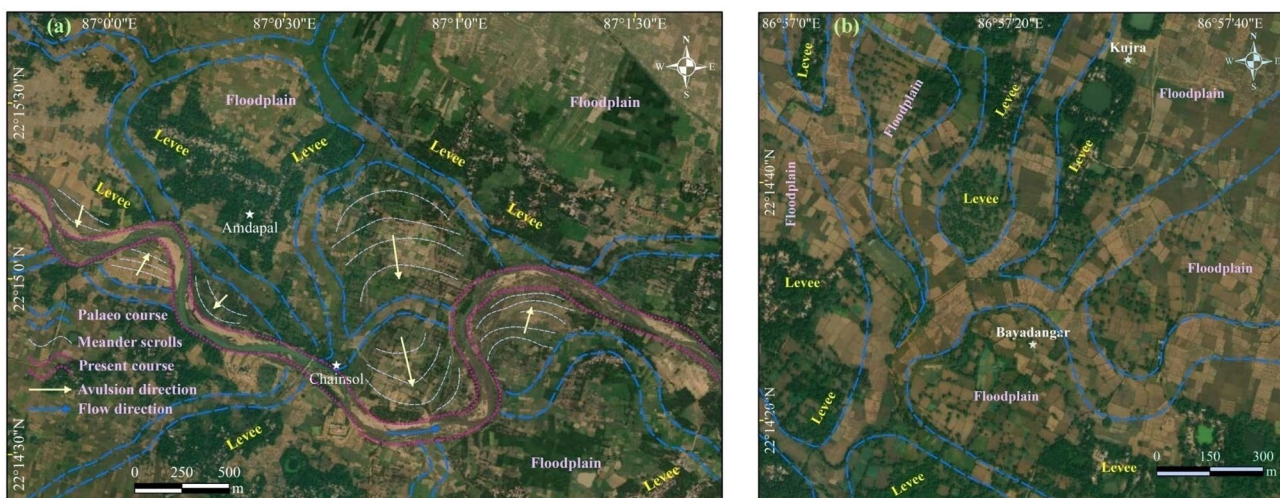


Fig. 10 Micro-level analysis of river adjustment and associated hydrogeomorphological features in the position of the 3rd stage of the river course shifting (denoted in Fig. 9b)

departing the previous course (Fig. 10a). However, the river also shifted towards the north in some positions under the hydrogeomorphological control at the local level. The micro-level study of the palaeo-channel pattern of stage 3 reveals that multiple branches have diverged from the mainstream and again converged together at a single stream before the confluence with Subarnarekha River (Fig. 10b). Such type of flow pattern is found over the very gentle gradient surface. The palaeo-courses were flowing from north to south and even north-east to south-west direction. Such type of flow pattern in the very gentle gradient surface also confers that the northeastern side of the lower basin area is raised to a certain extent.

Conclusion

The overall analysis of the river systems within the Dulung basin can be concluded that this area has been influenced by tectonic action and associated structural deformation. The north-west to south-east elongated basin has been formed during the lower Proterozoic to Quaternary period with composed of different hard rocks and soft sedimentary lithological structures. The existence of CFF and MFF faults respectively in the upper and lower ends of the basin coupled with the other tectonic evidence like basement faults, BGA, and earthquake epicenters around this region indicates the tectonic influence in the southwestern fringe of the Bengal Basin. Within 2100-m-thick sedimentary deposits over the basement of the Bengal Basin, the major changes of hydrogeomorphological variables and corresponding adjustments of river course have been associated in the higher tectonic potential areas in the upper, middle-lower and lower sections of the Dulung River system. The tectonic potential zones have been demarcated based on the analytical results of ten different parameters, i.e., basement depth, BGA, isobase, HG, lineament density, FTA, SI, PC-density, RDE-index, and T-index within the entire area.

The palaeo-channel patterns in the middle-lower and lower courses of the Dulung basin reveal the effects of tectonic influence and lithological variations. The present form of the drainage systems is contained into three sub-basins as the upper, middle, and lower basins. However, it was a single basin in the past and the river was confluence at the lower extent of the study area. The four stages of river adjustment are observed with their shifting course and confluences. The mainstreams of the earlier drainage systems were confluences with the Subarnarekha River (at different periods) near Dantan, Kulboni, Rohini, and in the upstream position of Ragra maintaining about 10–15-km inter-confluence distance. The pattern and positions of meander scrolls of the Subarnarekha River show that the river shifted towards the right (south). Moreover, the palaeo-channels also sharply turned towards the south before

confluences with the Subarnarekha River. The long profiles reveal that the river beds have been relatively elevated in the lower courses. The overall analysis of the palaeo-courses and their confluences reveals that the lower basin area raised around the MFF zone and the basin tilted southward, particularly in the middle and lower catchment areas. In this study, the relative positions and shifting of the river courses are estimated depending on the surface exposures of the hydrogeomorphological signatures. But the proper understanding of the chronological evolution of the Dulung River systems concerning the morphotectonic adjustment will be understood after the detailed study on the subsurface lithostratigraphic and dating records of different layers.

Acknowledgements The author is grateful to the United States Geological Survey (USGS) for making available the satellite images. The author is also immensely grateful to the Government of India for making available the Geological Quadrangle Map and Seismotectonic Atlas on Open Government Data (OGD) Platform free of charge. The author is thankful to Mr. Goutam Kumar Das, Mr. Chandan Maity, and Mr. Depal Bej for their laborious support during the course of fieldwork. The valuable suggestions from the anonymous reviewers on the manuscript are highly acknowledged.

Declarations

Conflict of interest The author declares that he has no competing interests.

References

- Adewumi AJ, Anifowose YB (2017) Hydrogeologic characterization of Owo and its environs using remote sensing and GIS. *Appl Water Sci* 7:2987–3000. <https://doi.org/10.1007/s13201-017-0611-8>
- Alexander J, Leeder MR (1987) Active tectonic control on alluvial architecture. In: Ethridge FG, Flores RM, Harvey MD (eds) *Recent Developments in Fluvial Sedimentology*. SEPM Special Publication, p 39:243–252
- Ambili V, Narayana AC (2014) Tectonic effects on the longitudinal profiles of the Chaliyar River and its tributaries, southwest India. *Geomorphology* 217:37–47. <https://doi.org/10.1016/j.geomorph.2014.04.013>
- Antón L, De Vicente G, Muñoz-Martín A, Stokes M (2014) Using river long profiles and geomorphic indices to evaluate the geomorphological signature of continental scale drainage capture, Duero basin (NW Iberia). *Geomorphology* 206:250–261. <https://doi.org/10.1016/j.geomorph.2013.09.028>
- Bera K, Bandyopadhyay J (2012) Ground water potential mapping in Dulung watershed using remote sensing & GIS techniques, West Bengal, India. *Int J Sci Res Publ* 2:1–7
- Calligaris C, Devoto S, Galve J, Zini L, Perez Pena JV (2017) Integration of multi-criteria and nearest neighbour analysis with kernel density functions for improving sinkhole susceptibility models: the case study of Enemonzo (NE Italy). *Int J Speleol* 46:191–204. <https://doi.org/10.5038/1827-806X.46.2.2099>
- Cox RT (1994) Analysis of drainage-basin symmetry as a rapid technique to identify areas of possible Quaternary tilt-block tectonics: an example from the Mississippi Embayment. *Geol Soc Am Bull* 106:571–581. [https://doi.org/10.1130/0016-7606\(1994\)106%3c0571:AODBSA%3e2.3.CO;2](https://doi.org/10.1130/0016-7606(1994)106%3c0571:AODBSA%3e2.3.CO;2)

- Dandapat K, Hazari R, Bhunia GS, Shit PK (2020) The Potential Gully Erosion Risk Mapping of River Dulung Basin, West Bengal, India Using AHP Method. In: Shit PK, Pourghasemi HR, Bhunia GS (eds) Gully erosion studies from India and surrounding regions. Springer, pp 93–107. https://doi.org/10.1007/978-3-030-23243-6_6
- Dar RA, Romshoo SA, Chandra R, Ahmad I (2014) Tectono-geomorphic study of the Karewa Basin of Kashmir Valley. *J Asian Earth Sci* 92:143–156. <https://doi.org/10.1016/j.jseae.2014.06.018>
- Earthquake Track (2020) Recent earthquakes near India. <https://earthquaketrack.com/p/india/recent>. Accessed 10 May 2020
- Etchebehere ML, Saad AR, Fulfaro VJ, de Jesus Perinotto JA (2004) Application of the “declivity-extension ratio – RDE” index in the Rio do Peixe basin (SP) to detect neotectonic deformations. *Geologia USP Série Científica* 4:43–56. <https://doi.org/10.5327/S1519-874X2004000200004>
- Etchebehere MLDC, Saad AR, Santoni G, da Costa Casado F, Fulfaro VJ (2006) Detection of probable neotectonic deformations in the Rio do Peixe valley, Western Paulista region, by application of RDE indices (declivity-extension relationship) in drainage segments. *Geociências (São Paulo)* 25:271–287
- Geological Survey of India (1998) Geological Quadrangle Map, Geological Survey of India, Government of India. https://www.gsi.gov.in/webcenter/portal/OCBIS/pageMAPS/pageMapsSeries?_adf.ctrl-state=wd51swrgt_5&_afLoop=27454911959312140#. Accessed 6 December 2015
- Geological Survey of India (2000) Seismotectonic Atlas of India and its Environs, Geological Survey of India, Government of India. <https://data.gov.in/catalog/digital-seismotectonic-atlas-india-and-its-environs>. Accessed 14 April 2020
- Golts S, Rosenthal E (1993) A morphotectonic map of the northern Arava in Israel, derived from isobase lines. *Geomorphology* 7:305–315. [https://doi.org/10.1016/0169-555X\(93\)90060-F](https://doi.org/10.1016/0169-555X(93)90060-F)
- Goodbred SL, Kuehl SA, Steckler MS, Sarkar MH (2003) Controls on facies distribution and stratigraphic preservation in the Ganges-Brahmaputra delta sequence. *Sed Geol* 155:301–316. [https://doi.org/10.1016/S0037-0738\(02\)00184-7](https://doi.org/10.1016/S0037-0738(02)00184-7)
- Grohmann CH (2004) Morphometric analysis in geographic information systems: applications of free software GRASS and R. *Comput Geosci* 30:1055–1067. <https://doi.org/10.1016/j.cageo.2004.08.002>
- Guha S, Patel PP (2017) Evidence of topographic disequilibrium in the Subarnarekha River Basin, India: a digital elevation model based analysis. *J Earth Syst Sci* 126(7):1–20
- Hare PH, Gardner TW (1985) Geomorphic indicators of vertical neotectonism along converging plate margins, Nicoya Peninsula, Costa Rica. In: Morisawa M, Hack JT (eds) *Tectonic Geomorphology*. Allen and Unwin, Boston, pp 75–104
- Holbrook J, Schumm SA (1999) Geomorphic and sedimentary response of rivers to tectonic deformation: a brief review and critique of a tool for recognizing subtle epeirogenic deformation in modern and ancient settings. *Tectonophysics* 305:287–306. [https://doi.org/10.1016/S0040-1951\(99\)00011-6](https://doi.org/10.1016/S0040-1951(99)00011-6)
- Horton RE (1932) Drainage basin characteristics. *Trans Am Geophys Union* 13:350–361
- Horton RE (1945) Erosional development of streams and their drainage basins: hydrophysical approach to quantitative morphology. *Geological Society of America Bulletin* 56:275–370
- Jacques PD, Salvador ED, Machado R, Grohmann CH, Nummer AR (2014) Application of morphometry in neotectonic studies at the eastern edge of the Paraná Basin, Santa Catarina State, Brazil. *Geomorphology* 213:13–23. <https://doi.org/10.1016/j.geomorph.2013.12.037>
- Jana S (2019) An automated approach in estimation and prediction of riverbank shifting for flood-prone middle-lower course of the Subarnarekha River, India. *International Journal of River Basin Management*. <https://doi.org/10.1080/15715124.2019.1695259>
- Jana S (2020) Micro-level coastal vulnerability assessment in relation to post-Aila landscape alteration at the fragile coastal stretch of the Sagar Island, India. *Reg Stud Mar Sci*. <https://doi.org/10.1016/j.rsma.2019.100908>
- Jana S, Paul AK (2019) Assessment of morphogenetic sedimentary depositional environments of different morphological surfaces of middle-lower and deltaic courses of Subarnarekha River. *Journal of Coastal Sciences* 6:1–11
- Jozi SA, Rezaeian S, Saei F (2017) Study of morphologic changes in Karun River using linear directional mean, remote sensing and geographic information system. *International Journal of Urban Management and Energy Sustainability* 1:71–78. <https://doi.org/10.22034/IJUMES.2017.01.01.007>
- Kale VS, Sengupta S, Achyuthan H, Jaiswal MK (2014) Tectonic controls upon Kaveri River drainage, cratonic Peninsular India: Inferences from longitudinal profiles, morphotectonic indices, hanging valleys and fluvial records. *Geomorphology* 227:153–165. <https://doi.org/10.1016/j.geomorph.2013.07.027>
- Keller EA, Pinter N (1996) *Active tectonics: earthquakes, uplift and landscape* (1st edition). Prentice Hall, New Jersey, p 156
- Keller EA, Pinter N (2002) *Active tectonics: earthquakes, uplift, and landscape* (2nd edition). Prentice Hall, New Jersey, pp 1–362
- Kirby E, Whipple KX (2012) Expression of active tectonics in erosional landscapes. *J Struct Geol* 44:54–75. <https://doi.org/10.1016/j.jsg.2012.07.009>
- Leopold LB, Wolman MG, Miller JP (1964) *Fluvial processes in geomorphology*. Freeman, San Francisco, CA, p 522
- Lindenschmidt KE, Long J (2013) A GIS approach to define the hydrogeomorphological regime for instream flow requirements using geomorphic response units (GRU). *River Systems* 20:261–275. <https://doi.org/10.1127/1868-5749/2012/0053>
- Luirei K, Bhakuni SS, Kothari GC (2015) Drainage response to active tectonics and evolution of tectonic geomorphology across the Himalayan Frontal Thrust, Kumaun Himalaya. *Geomorphology* 239:58–72. <https://doi.org/10.1016/j.geomorph.2015.03.011>
- Mandal A, Mohanty WK, Sharma SP, Biswas A, Sen J, Bhatt AK (2015) Geophysical signatures of uranium mineralization and its subsurface validation at Beldih, Purulia District, West Bengal, India: a case study. *Geophys Prospect* 63:713–726. <https://doi.org/10.1111/1365-2478.12205>
- Marghany M, Hashim M (2010) Lineament mapping using multi-spectral remote sensing satellite data. *International Journal of Physical Sciences* 5:1501–1507. <https://doi.org/10.3923/rjasci.2010.126.130>
- Miller JR (1991) The influence of bedrock geology on knickpoint development and channel-bed degradation along downcutting streams in south-central Indiana. *J Geol* 99:591–605. <http://www.jstor.com/stable/30065004>. Accessed 12 Sept 2020
- Miller SR, Baldwin SL, Fitzgerald PG (2012) Transient fluvial incision and active surface uplift in the Woodlark Rift of eastern Papua New Guinea. *Lithosphere* 4:131–149. <https://doi.org/10.1130/L135.1>
- Miller VC (1953) A quantitative geomorphic study of drainage basin characteristics in the Clinch Mountain area, Virginia and Tennessee. Project NR 389042, Tech Rept. 3, Columbia University, Department of Geology, ONR Geography Branch, New York, p 25
- Mokarrama M, Hojati M (2018) Landform classification using a sub-pixel spatial attraction model to increase spatial resolution of digital elevation model (DEM). *Egyptian Journal of Remote Sensing and Space Science* 21:111–120. <https://doi.org/10.1016/j.ejrs.2016.11.005>
- Mondal SK, Jana S, Majumder M, Roy D (2012) A comparative study for prediction of direct runoff for a river basin using geomorphological approach and artificial neural networks. *Appl Water Sci* 2:1–13. <https://doi.org/10.1007/s13201-011-0020-3>

- Moussi A, Rebai N, Chaieb A, Saadi A (2018) GIS-based analysis of the Stream Length-Gradient Index for evaluating effects of active tectonics: a case study of Enfidha (North-East of Tunisia). *Arab J Geosci* 11:123. <https://doi.org/10.1007/s12517-018-3466-x>
- Mukul M, Jade S, Ansari K, Matin A (2014) Seismotectonic implications of strike-slip earthquakes in the Darjiling–Sikkim Himalaya. *Curr Sci* 106:198–210
- Mwaniki MW, Moeller MS, Schellmann G (2015) A comparison of Landsat 8 (OLI) and Landsat 7 (ETM+) in mapping geology and visualising lineaments: a case study of central region Kenya. In: *The International Archives of the Photogrammetry, Remote Sensing and Spatial Information Sciences*, vol XL-7/W3. 36th International Symposium on Remote Sensing of Environment 11–15 May 2015. Berlin, pp 897–903 Germany. <https://doi.org/10.5194/isprsarchives-XL-7-W3-897-2015>
- Nath SK, Adhikari MD, Maiti SK, Devaraj N, Srivastava N, Mohapatra LD (2014) Earthquake scenario in West Bengal with emphasis on seismic hazard microzonation of the city of Kolkata, India. *Nat Hazard* 14:2549. <https://doi.org/10.5194/nhess-14-2549-2014>
- NRSC (2014) National Geomorphological and Lineament Mapping on 1:50,000 Scale using Resourcesat-1 LISS-III Data. Manual for Geomorphology and Lineament Mapping (Web Version). National Remote Sensing Centre, Hyderabad, India
- Patel A, Katiyar SK, Prasad V (2016) Performances evaluation of different open source DEM using differential global positioning system (DGPS). *Egyptian Journal of Remote Sensing and Space Science* 19:7–16. <https://doi.org/10.1016/j.ejrs.2015.12.004>
- Patel PP, Sarkar A (2009) Application of SRTM data in evaluating the morphometric attributes: a case study of the Dulung River Basin. *Practical Geography* 13:249–265
- Patel PP, Sarkar A (2010) Terrain characterization using SRTM data. *Journal of Indian Society of Remote Sensing* 38:11–24. <https://doi.org/10.1007/s12524-010-0008-8>
- Perez-Pena JV, Azor A, Azanon JM, Keller EA (2010) Active tectonics in the Sierra Nevada (Betic Cordillera, SE Spain): insights from geomorphic indexes and drainage pattern analysis. *Geomorphology* 119:74–87. <https://doi.org/10.1016/j.geomorph.2010.02.020>
- Philip GM, Watson DF (1982) A precise method for determining contoured surfaces. *J Aust Petrol Explor Assoc* 22:205–212. <https://doi.org/10.1071/AJ81016>
- Rao KN, Subrauel P, Nagakumar KCV, Demudu G, Malini BH, Rajawat AS (2013) Geomorphological implications of the basement structure in the Krishna-Godavari deltas, India. *Zeitschrift Fur Geomorphologie* 57:25–44. <https://doi.org/10.1127/0372-8854/2012/0076>
- Rhoads BL, Riley JD, Mayer DR (2009) Response of bed morphology and bed material texture to hydrological conditions at an asymmetrical stream confluence. *Geomorphology* 109:161–173. <https://doi.org/10.1016/j.geomorph.2009.02.029>
- Roy D, Begam S, Ghosh S, Jana S (2013) Calibration and validation of HEC-HMS model for a river basin in Eastern India. *ARNP Journal of Engineering and Applied Sciences* 8:40–56
- Roy S, Sahu AS (2015) Quaternary tectonic control on channel morphology over sedimentary low land: a case study in the Ajay-Damodar interfluvium of Eastern India. *Geosci Front* 6:927–946. <https://doi.org/10.1016/j.gsf.2015.04.001>
- Roy S, Sahu AS (2016) Morphotectonic map generation using geoinformatics technology: case study over the Ajay-Damodar Interfluvium, West Bengal, INDIA. *Arab J Geosci* 9:183. <https://doi.org/10.1007/s12517-015-2247-z>
- Saha D, Das D, Dasgupta R, Patel PP (2020) Application of ecological and aesthetic parameters for riparian quality assessment of a small tropical river in eastern India. *Ecol Ind* 117. <https://doi.org/10.1016/j.ecolind.2020.106627>
- Sahu S, Raju NJ, Saha D (2010) Active tectonics and geomorphology in the Sone-Ganga alluvial tract in mid-Ganga Basin, India. *Quatern Int* 227:116–126. <https://doi.org/10.1016/j.quaint.2010.05.023>
- Salvany JM (2004) Tilting neotectonics of the Guadimar drainage basin, SW Spain. *Earth Surf Proc Land* 29:145–160. <https://doi.org/10.1002/esp.1005>
- Sarkar A, Patel PP (2011) Topographic analysis of the Dulung River Basin. *Indian Journal of Spatial Science* 2:19
- Sarkar A, Patel PP (2012) Terrain classification of the Dulung drainage basin. *Indian Journal of Spatial Science* 3:1–8
- Sarkar A, Patel PP (2017) Land use-terrain correlations in the piedmont tract of Eastern India: a case study of the Dulung River Basin. In: Santra A, Mitra SS (eds) *Remote Sensing Techniques and GIS Applications in Earth and Environmental Studies*, pp 147–192. <https://doi.org/10.4018/978-1-5225-1814-3.ch008>
- Sboras S, Ganas A, Pavlides S (2010) Morphotectonic analysis of the neotectonic and active faults of Beotia (Central Greece), using G.I.S. Techniques. *Bull Geol Soc Greece* 43:1607–1618. <https://doi.org/10.12681/bgsg.11335>
- Schumm SA (1956) Evolution of drainage systems and slopes in badlands at Perth Amboy, New Jersey. *Geol Soc Am Bull* 67:597–646. [https://doi.org/10.1130/0016-7606\(1956\)67\[597:EODSAS\]2.0.CO;2](https://doi.org/10.1130/0016-7606(1956)67[597:EODSAS]2.0.CO;2)
- Schumm SA (1981) Evolution and response of the fluvial system, sedimentologic implications. In: Ethridge FG, Flores RM (eds) *Recent and ancient nonmarine depositional environments*. SEPM Special Publication, 31 pp 19–29
- Schumm SA, Dumont JF, Holbrook JM (2000) *Active tectonics and alluvial rivers*. Cambridge University Press, Cambridge, p 276
- Sharma HS (1979) *The physiography of the lower Chambal valley and its agricultural development: a study in applied geomorphology*. Concept, New Delhi, p 243
- Siddiqui S (2014) Appraisal of active deformation using DEM-based morphometric indices analysis in Emilia-Romagna Apennines, Northern Italy. *Geodynamics Research International Bulletin* 1:XXXIV–XLII
- Silva PG, Goy JL, Zazo C, Bardaji T (2003) Fault-generated mountain fronts in southeast Spain: geomorphologic assessment of tectonic and seismic activity. *Geomorphology* 50:203–225. [https://doi.org/10.1016/S0169-555X\(02\)00215-5](https://doi.org/10.1016/S0169-555X(02)00215-5)
- Strahler AN (1964) Quantitative geomorphology of drainage basins and channel networks. Section 4-II. In: Chow VT (ed) *Handbook of Applied Hydrology*. McGraw-Hill, New York, pp 4–39
- Toudeshki VH, Arian M (2011) Morphotectonic analysis in the Ghezeli Ozan river basin, NW Iran. *Journal of Geography and Geology* 3:258–265. <https://doi.org/10.5539/jgg.v3n1p258>
- United State Geological Society (1997) *Introduction to potential fields: gravity*. FS-239–95. Available on. <http://pubs.usgs.gov/fs/fs-0239-95/fs-0239-95.pdf>. Accessed 21 April 2020
- Verrios S, Zygouri V, Kokkalas S (2004) Morphotectonic analysis in the Eliki fault zone (Gulf of Corinth, Greece). *Bull Geol Soc Greece* 36:1706–1715. <https://doi.org/10.12681/bgsg.16578>
- Whittaker AC (2012) How do landscapes record tectonics and climate? *Lithosphere* 4:160–164. <https://doi.org/10.1130/RF.L003.1>
- Wobus CW, Whipple KX, Kirby E, Snyder NP, Johnson J, Spyropolou K, Crosby BT, Sheehan D (2006) Tectonics from topography: Procedures, promise and pitfalls. In: Willett SD, Hovius N, Brandon MT, Fisher DM (eds) *Tectonics, Climate and Landscape Evolution: Special Papers-Geological Society of America* 398, Penrose Conference Series, pp 55–74. [https://doi.org/10.1130/2006.2398\(04\)](https://doi.org/10.1130/2006.2398(04))